Multi-scale modeling of the North Pacific Ocean: Assessment and analysis of simulated basin-scale variability (1996–2003)

Enrique N. Curchitser,[1] Dale B. Haidvogel,[2] Albert J. Hermann,[3] Elizabeth L. Dobbins,[3] Thomas M. Powell,[4] and Alexey Kaplan[1]

Received 29 January 2005; revised 9 June 2005; accepted 18 August 2005; published 30 November 2005.

[1] A primitive equation ocean general circulation model is used to investigate climate impacts in the North Pacific Ocean in the 1996 to 2003 period. The objective is to assess the model ability to reproduce observed modes of variability and study their impact in the northeast Pacific. This work is done within the framework of the U.S. Global Ecosystem (GLOBEC) Northeast Pacific Program studying the links between climate variability and ecosystem dynamics. Three large-scale events are considered: The 1997/1998 El Niño, the 1999 "regime shift," and the 2002 cold/fresh subsurface anomalous water mass that was observed in the Gulf of Alaska and off the coast of Oregon. The circulation model is shown to generate the correct seasonal to interannual large-scale variability and is able to represent the climatic signals of interest in the eastern Pacific. We show that the influence of the 1997/1998 El Niño reached the coastal Gulf of Alaska and induced an increase in the upper ocean heat content along the coast of North America. An analysis of the sea surface temperature for the model years shows agreement between model and data in the representation of the 1999 shift to a cold phase in the eastern and northern North Pacific. Finally, using the model results, we speculate that the origin of the 2002 cold/fresh anomaly in the northeast Pacific was due to enhanced mixing during the preceding winter in the center of the Alaska gyre. Owing to anomalous changes in the density structure of the upper ocean, this water was able to move geostrophically toward the coast and it persisted in the northeast Pacific below the mixed layer the following year.

Citation: Curchitser, E. N., D. B. Haidvogel, A. J. Hermann, E. L. Dobbins, T. M. Powell, and A. Kaplan (2005), Multi-scale modeling of the North Pacific Ocean: Assessment and analysis of simulated basin-scale variability (1996–2003), *J. Geophys. Res.*, *110*, C11021, doi:10.1029/2005JC002902.

1. Introduction

[2] Regional ecosystem variability is an integrated response to local/short- and basin/climate-scale changes. Ecosystem dynamics have been linked to local topographic and coastal features and mesoscale activity, as well as to long-term and basin-scale ocean states and interannual changes caused by phenomena such as the El Niño–Southern Oscillation. One of the main challenges is to understand the cumulative effects of the large- and regional-scale physics on ecosystem dynamics and variability.

[3] The context for the current work is the U.S. Global Ecosystem Dynamics Northeast Pacific Program (GLOBEC-NEP). U.S. GLOBEC is a multidisciplinary research program designed to determine the potential impact of global climate change on ocean ecosystems. The objective of U.S. GLOBEC research is to understand how climate change and variability translate into changes in the structure and dynamics of marine ecosystems and in fisheries production.

[4] GLOBEC studies are ongoing in several key locations, including the northwest Atlantic, the northeast Pacific, and the Southern Ocean, where the effects of changes in ocean currents, circulation patterns, upwelling (and downwelling) processes, stratification and front formation, and sea ice extent can be studied in detail. Research sites have been specifically chosen to afford opportunities to study one or more of these processes and their effects on selected species. GLOBEC research encompasses newly developed technologies for sampling, developing of coupled physical-biological models, conducting process-oriented observational studies to obtain key parameter estimates, and undertaking retrospective studies to provide insights based on observations carried out over broad time and space scales.

[5] The physical setting for the Northeast Pacific GLOBEC program is the eastern extent of the subarctic

[1]Lamont Doherty Earth Observatory of Columbia University, Palisades, New York, USA.
[2]Institute of Marine and Coastal Sciences, Rutgers University, New Brunswick, New Jersey, USA.
[3]Pacific Marine Environmental Laboratory–NOAA/Joint Institute for the Study of the Atmosphere and the Ocean, University of Washington, Seattle, Washington, USA.
[4]Department of Integrative Biology, University of California at Berkeley, Berkeley, California, USA.

0148-0227/05/2005JC002902$09.00

and subtropical gyres formed by the bifurcation of the North Pacific Current (also referred to as the West Wind Drift) as it nears the western coast of North America. The two distinct circulation features are the Alaskan Current–Alaskan Stream System and the California Current System. In these two regions, physical and biological variables have been shown to be strongly correlated over temporal scales ranging from seasonal to decadal [*Batchelder and Powell*, 2002; *Ware and Thomson*, 2000]. Furthermore, there is evidence that both the physics and biology of the region respond to the mesoscale and large scale as well as to seasonal to interdecadal variability. Ocean variability can be measured by seasonal/interannual/decadal changes in sea surface height/temperature, transport in the coastal currents, mixed layer depth, location of gyres boundaries, etcetera. Biological and ecosystem changes are often measured in terms of species selection, biomass abundance and geographic distribution of particular species across trophic levels.

[6] The most prominent example of interannual ocean variability in the North Pacific is the El Niño–Southern Oscillation (ENSO) phenomena. Though its effects are most pronounced in the equatorial Pacific, the ENSO signal does propagate poleward to the extratropics (both via atmospheric teleconnections and the oceanic waveguide) and significant changes are observed as far north as the Gulf of Alaska. In the northeast Pacific region, changes in sea surface temperatures and height and alongshore transports have been associated with ENSO events [*Royer*, 1985; *Huyer and Smith*, 1985; *Huyer et al.*, 2002]. The local biogeochemistry is sensitive to these physical changes; for example, enhanced alongshore advection can change the faunal community composition found at a given latitude. Variability in upwelling/downwelling rates affects the nutrient supply in a given ecosystem. Other scales of spatial and temporal variability are the coupled physical/biological changes due to mesoscale features [*Powell et al.*, 2005] and the interdecadal basin-scale regime shifts [*Bond et al.*, 2003; *Hare and Francis*, 1995; *Mantua et al.*, 1997].

[7] The objective of the current paper is to assess and analyze the simulated basin-scale variability in the North Pacific Ocean within the context of the GLOBEC-NEP program. We therefore choose the time period for the simulations that coincides with the extensive field program both in the California Coastal Current and the Coastal Gulf of Alaska, the late 1990s and early 2000s. The analysis is concentrated on events that have been linked to variability in the ecosystems of each of the target regions: the 1997–1998 El Niño, the late 1990s shift to cooler surface waters in the eastern and subpolar Pacific, and the 2002 subsurface cold anomaly in the northeast Pacific. The overarching questions are as follows. (1) How well can a forced circulation model reproduce these events? (2) What are the regional physical signatures of these large-scale events? (3) What are the mechanisms that induce the regional physical variability?

[8] *Strub and James* [2002] describe the evolution of the strong 1997–1998 El Niño and its effect on the circulation in the California Current and the Alaska Gyre using TOPEX/Poseidon satellite altimetry. They find that two distinct pulses of high sea level propagated poleward along the North American coast. The first one, during the spring-summer of 1997, stalled around 23–24°N, and the second, during the fall-winter of 1997–1998, reached at least as far as the Canadian border by late May of 1998, aided by anomalous poleward wind forcing. A response to changes in the basin-scale winds is suggested as the main cause for variability in the basin interior and the North Pacific current. The most significant response to the oceanic signal was limited to the coastal and equatorial waveguides. Correlation coefficients for sea surface height varied from 0.86 between southern Mexico and California to 0.61 when comparing to southern Alaska/British Columbia. Observations along the North Pacific eastern boundary during the El Niño event suggest an anomalous poleward transport resulting in warmer, saltier subsurface waters [*Kosro*, 2002; *Dever and Winant*, 2002; *Durazo and Baumgartner*, 2002].

[9] Analysis of sea level pressure and sea surface temperature (SST) anomalies during the winters of 1999–2002 reveal patterns unlike those of the leading North Pacific climate variability pattern, the Pacific Decadal Oscillation (PDO [*Bond et al.*, 2003]). During these winters, the North Pacific Ocean was subject to a forcing pattern reminiscent of that before the 1976/1977 regime shift. The new state is characterized by an SST cold anomaly that extends from the waters off California across the Pacific (north of 40°N) to the Sea of Okhotsk, and a warm anomaly south of 40°N extending from Asia to about 150°W. This new pattern coincides with an observed new climate regime in northeast Pacific ecosystems [*Peterson and Schwing*, 2003]. The analysis carried out by *Bond et al.* [2003] reveals that the new state of the North Pacific can be described by the second principal component (PC) and corresponding empirical orthogonal function (EOF) of winter sea surface temperature anomalies and is uncorrelated with the PDO which is represented by the first PC/EOF pair. Physical and ecosystem responses to the new patterns are geographically dependent. Observations in the northeast Pacific [*North Pacific Marine Science Organization* (*PICES*), 2005] indicate a cooling of the coastal waters in the California Current System, a deepening of the thermocline and decreased stratification. A deepening of the mixed layer was observed in the Gulf of Alaska while no apparent response was observed in the Bering Sea.

[10] Measurements off the coast of Oregon and Vancouver Island in the summer of 2002 reveal an anomalously cold and fresh subsurface layer that coincides with the permanent halocline and a possible increase in biological productivity [*Freeland et al.*, 2003]. This layer is about 100 m thick and lies roughly between 30 and 150 m depth. When compared with June–July means in 2001, the 2002 waters reached temperatures of more than 1°C cooler and salinities of 0.4 psu fresher. *Freeland et al.* [2003] suggest various mechanisms that could contribute to this cold anomaly, among them are anomalous alongshore and zonal advection, Ekman transport, upwelling/downwelling, and enhanced winter mixing. Given the lack of a clear connection to changes in any of the relevant climate indices for the North Pacific (e.g., the Pacific Decadal Oscillation, the North Pacific Index), they speculate that the cold anomaly may be a coincidence of some of the above-mentioned mechanisms. *Crawford et al.* [2005] analyze data derived from the Argo floats in the Gulf of Alaska (Project Argo: A global array of profiling floats, available from the Argo science team at http://www-argo.ucsd.edu/ArgoBrouchure.

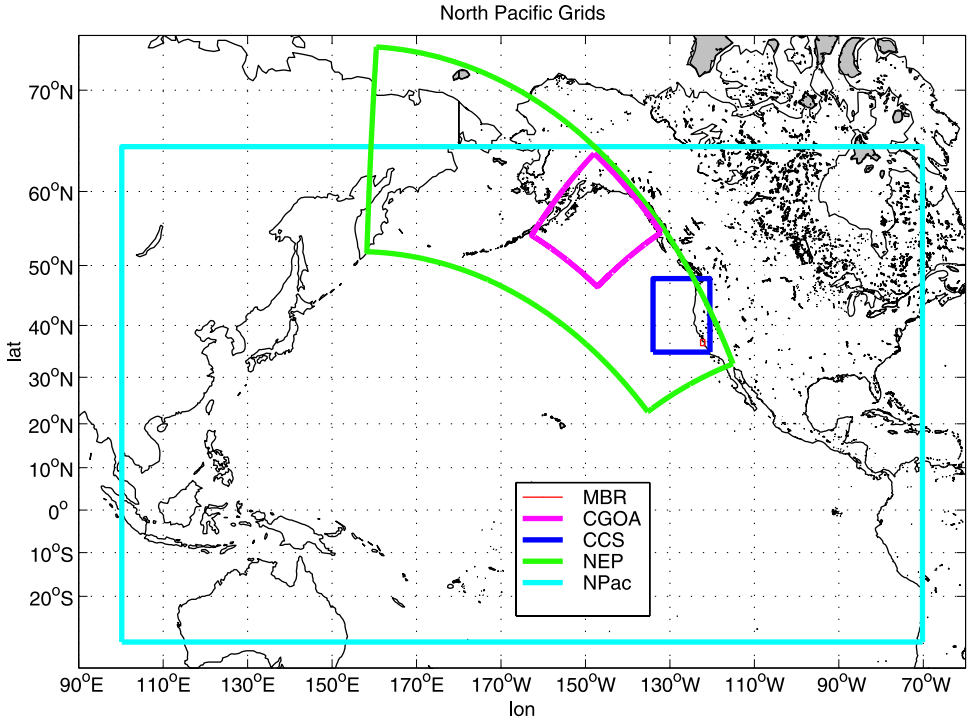

Figure 1. North Pacific nested grids setup. Approximate resolutions are: NPac, 0.4°; NEP, 10 km; CCS and CGOA, 2–3 km; MBR (Monterey Bay Region), 250 m.

pdf) and see evidence of a steady, anomalously cold eastward flow in the halocline below the mixed layer. They speculate that this waters may have formed during the winter time in the center of the Alaska Gyre.

[11] The rest of the paper is organized as follows: In section 2, we describe the model setup including descriptions of the model, the grid for the North Pacific simulation and the forcing data. In section 3, we describe the spinup and low-frequency model behavior; section 4 describes the basin-scale model response for the hindcast simulations, and in sections 5, 6 and 7 we present an analysis for the 1997/1998 El Niño, the regime shift and the 2002 cold anomaly, respectively. Concluding remarks and future directions are presented in section 8.

2. Methodology

[12] The range of temporal and spatial scales relevant to ocean circulation presents a technical challenge that we address with a multi-scale modeling approach; basin-scale simulations are used to investigate large-scale and long-term variability, and regional models are used to study high-resolution and relatively short-duration phenomena.

[13] In order to address the stated goals of the GLOBEC program, a suite of nested computational domains was implemented, extending from the basin scale to the coastal regions of interest. The outline of the computational grids is shown in Figure 1. The basin-scale North Pacific grid (NPac) has a nominal resolution of 0.4°, the intermediate northeast Pacific (NEP) has a resolution of 10 km, and the coastal California Coastal Current (CCS) and Coastal Gulf of Alaska (CGOA) has a resolution of 2–3 km. The NPac domain is used to simulate the basin-scale ocean circulation variability that results from climate-scale (temporal and spatial) forcing signals such as the El Niño/Southern Oscillation and changes associated with the Pacific Decadal Oscillation (PDO) index. A gradual downscaling of the basin-scale signal is achieved by generating initial and boundary conditions from NPac, and thereafter used by the intermediate NEP model which is run for a time period concurrent with NPac. Finally, a similar downscaling is performed from NEP to either the CCS or the CGOA domains. The high-resolution domains are designed to simulate the mesoscale variability in the respective regions in response to both local-scale (atmospheric and riverine) and basin-scale (through the boundary conditions) forcing. Owing to time step limitations, the high-resolution domains are considerably more expensive to run and therefore the finest regional simulations are presently limited to periods that coincide with the GLOBEC field seasons (2000 and 2002 for CCS, 2001 and 2003 for CGOA). Results from the inner-nested domains will be discussed in future separate publications.

[14] The ocean circulation model used for this work is the Regional Ocean Modeling System (ROMS) [*Shchepetkin and McWilliams*, 1998, 2003; *Song and Haidvogel*, 1994]. The dynamical core is based on the free-surface, hydrostatic primitive equations of ocean circulation. The model employs a nonlinear stretched vertical coordinate that follows the bathymetry and the free surface; the horizontal space is discretized using orthogonal curvilinear coordinates on an Arakawa C-grid. A robust and accurate pressure gradient discretization with a reformulated equation of state achieve significantly reduced pressure gradients errors compared to traditional terrain-following coordinate models. Split-explicit time stepping of the barotropic/baroclinic

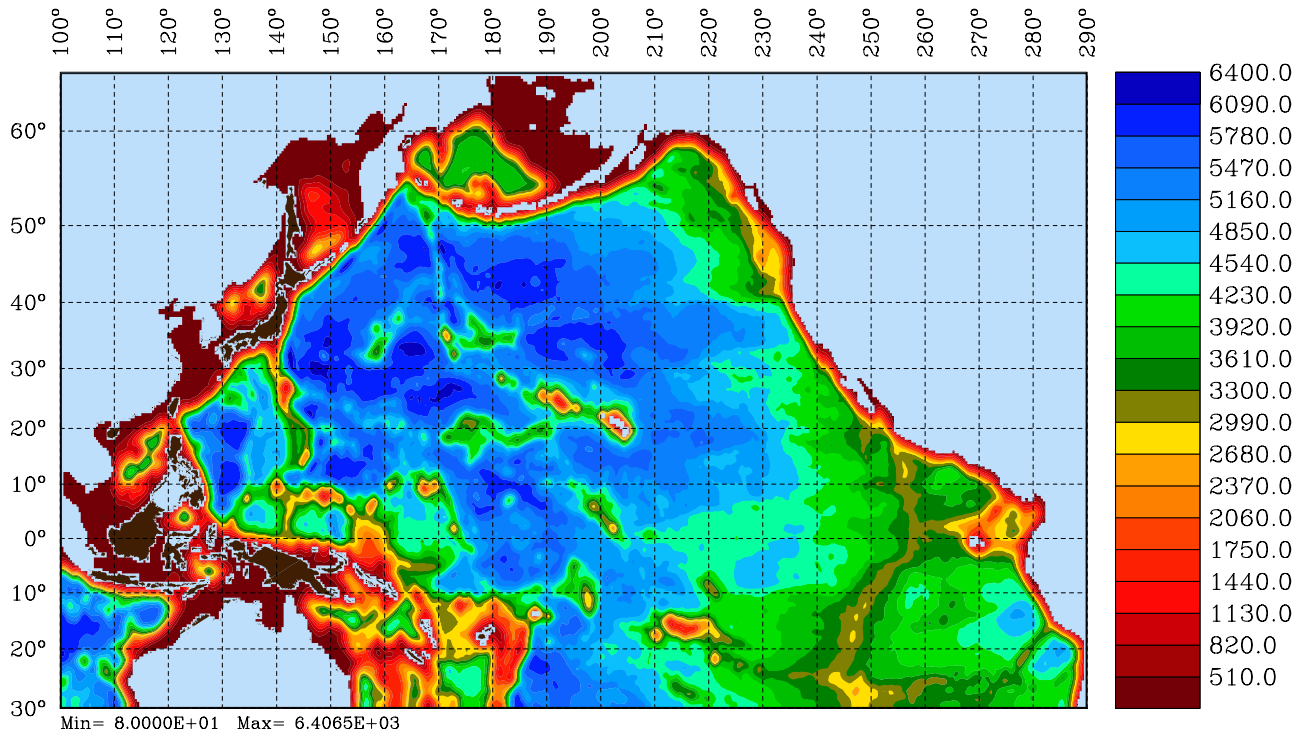

Figure 2. NPac: ETOPO5 model bathymetry (meters).

modes is formulated so as to maintain both volume conservation and constancy preservation properties. A third-order upstream-biased advection operator reduces dispersive errors and minimizes dissipation, effectively increasing the resolution on a given grid.

[15] The available suite of sub-grid space parameterizations include the K-Profile Parametrization [KPP; *Large et al.* 1994], Mellor-Yamada 2.5 [*Mellor and Yamada*, 1982], and the Generic Length Scale (GLS) [*Umlauf and Burchard*, 2005] encompassing $k - \epsilon$, $k - \omega$ and Mellor-Yamada closures for the mixed layer. Bottom drag can be represented by either linear or quadratic formulations; horizontal diffusion and dissipation can be parameterized with either Laplacian or bi-harmonic operators. A bulk-flux treatment for the air-sea exchange is based formulation of *Fairall et al.* [1996b].

[16] A salient feature of ROMS is the advanced treatment of open boundary conditions permitting stable, long-duration, high-resolution limited-area simulations and the downscaling of basin-scale signals to regional domains. The ROMS open boundary condition formulation is based on tracer and momentum exchanges on the grid interface and, where appropriate, an oblique radiation scheme with a differential restoring timescale correlated with the direction of information flow in or out of a domain [*Marchesiello et al.*, 2001].

[17] Other system attributes include extensive restructuring for sustained performance on parallel-computing platforms; high-order, weakly dissipative algorithms for tracer advection and an integrated set of procedures for data assimilation (e.g., optimal interpolation, reduced-state Kalman filter, and adjoint-based methods). Further numerical details are given by *Moore et al.* [2004], *Shchepetkin and McWilliams* [1998, 2003, 2005], and *Warner et al.* [2005], and on the ROMS web site (http://www.marine.rutgers.edu/po/).

[18] The North Pacific basin model domain used for this work ranges from 30°S to 65°N and from 100°E to 290°E in latitude and longitude, respectively. The average horizontal grid spacing is approximately 0.4°, and 30 vertical layers are used. The resulting grid has 476 × 238 × 30 points. Following the notation of *Song and Haidvogel* [1994] for the stretched generalized terrain-following coordinates, we use values of $\theta_s = 5$ and $\theta_b = 0.4$ resulting in a vertical distribution of grid points that is enhanced in the surface and benthic boundary layers. The baroclinic and barotropic time steps are 1600 and 36 s, respectively. Vertical mixing is determined by the KPP scheme. As a consequence of implicit scale-selective smoothing in the third-order upwind advection scheme, no explicit horizontal dissipation or diffusion are needed. A nondimensional quadratic bottom drag coefficient of 3×10^{-3} is used. The model bathymetry is interpolated from *ETOPO5* [1988] (see Figure 2), with a minimum depth set to 40 m. An attempt was made to keep isobaths from intersecting side walls and to keep shallow areas intact. Nevertheless, at the current resolution, the shelf areas are poorly resolved and topographic smoothing creates significant discrepancies. For the current set of simulations, the boundary conditions are no-slip closed walls. Tides and riverine inputs are omitted in these computations, though they are included in the high-resolution simulations using the northeast Pacific (NEP) grid, the coastal Gulf of Alaska (CGOA) and the California Coastal Current System (CCS) (see Figure 1).

[19] The three numerical experiments in the NPac domain described in this paper are a climatological spin-up and two hindcast simulations. For the spin-up phase (also referred to as run S-C) the model is initialized from rest with Levitus

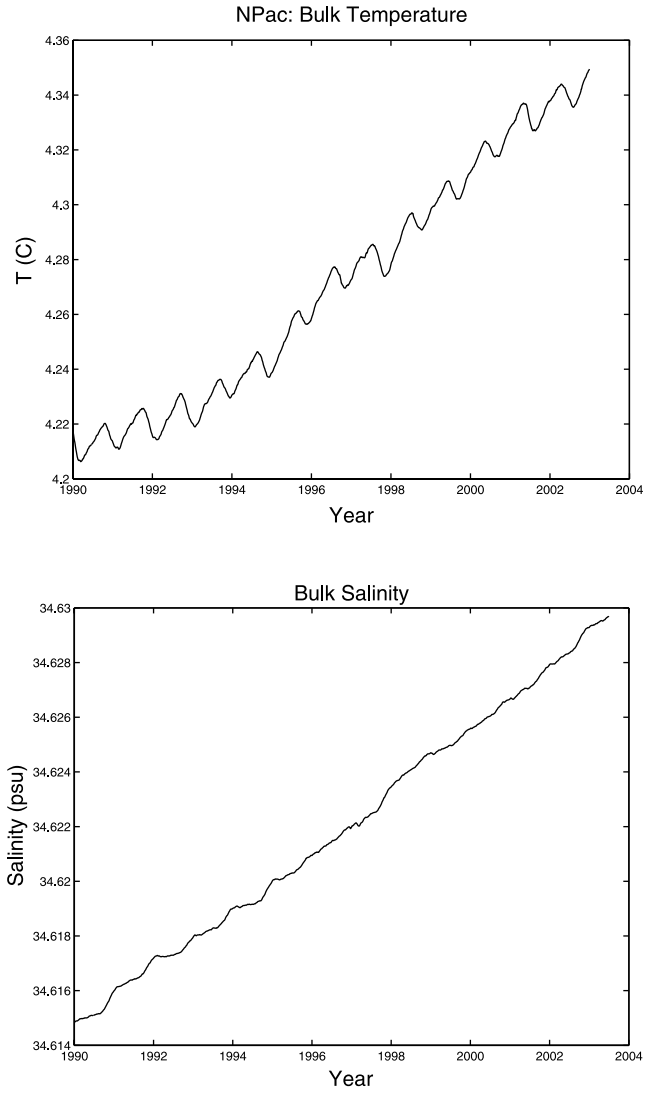

Figure 3. Bulk (top) temperature and (bottom) salinity drifts.

January climatology in the upper 1500 m and yearly values at depth [*Levitus and Boyer*, 1994; *Levitus et al.*, 1994]. The surface forcing is obtained from COADS monthly fluxes [*DaSilva et al.*, 1994]. The climatological spin-up computation is carried out for a period of 10 years to allow the transients associated with the impulsive start to subside and the circulation to reach a quasi-steady energy level. The first hindcast simulation (run H-N) is for the period of 1990–2003 and is initialized from the end of the spin-up run. The forcing is derived from NCAR/NCEP daily reanalysis wind and flux products [*Kalnay et al.*, 1996]. The model employs a bulk-flux formulation [*Fairall et al.*, 1996a, 1996b] to compute the surface fluxes. No surface restoring is used. Finally a second hindcast simulation (run H-Q) is performed for the period of 2000–2002 employing QuikSCAT-derived winds [*Wentz et al.*, 2001; *Bourassa et al.*, 2003] with all other forcing aspects equivalent to run H-N. Run H-Q is initialized from the 1 January 2000 averaged output of run H-N. QuikSCAT data are available beginning January 2000. The model output consists of 3-day averages of all prognostic and some diagnostic variables (e.g., boundary layer depth and vertical mixing coefficients).

3. Spin-up and Low-Frequency Model Behavior

[20] The climatological spin-up is used to set up the large-scale context for the hindcast simulations and to assess model drift. Following the impulsive start, geostrophic adjustment results in a three-dimensional circulation which is in balance with the temperature and salinity fields imposed by the initial conditions. Once the model evolves through the initial transients, the circulation reaches a slowly varying equilibrium with the prescribed atmospheric forcing. The monthly climatology used in the forcing permits the model to establish a quasi-steady state and set up a seasonal progression of phenomenology. Specific temporal variability is added to the forcing to produce a hindcast simulation.

[21] The climatological spin-up simulation (S-C) serves two purposes: The first is to allow the model to evolve through the transients resulting from the abrupt initialization and the second is to quantify model drift. The latter can only be achieved in a climatological experiment with no interannual variability in the forcing. It is also important to investigate the low-frequency behavior of the hindcast simulations. The expectation is that during a decade of a basin-scale simulation the bulk drift from climatology will be small relative to interannual and seasonal changes.

[22] Using the output from the spin-up run as an initial condition, the hindcast simulation was performed for the period of 1990–2003. The implemented bulk-flux formulation for the surface forcing has a feedback mechanism for adjusting the sensible heat flux to match the model sea surface temperature with the prescribed atmospheric boundary layer air temperature. Figure 3 shows the evolution of the bulk model temperature and salinity ($\overline{T}^{xyz}$), ($\overline{S}^{xyz}$) throughout the hindcast simulation. Over the 13 years of simulation the average temperature in NPac rose from 4.22° to 4.35°C, or an average of 0.01°C per simulation year. The salinity rose from 36.615 to 36.63 psu amounting to a drift

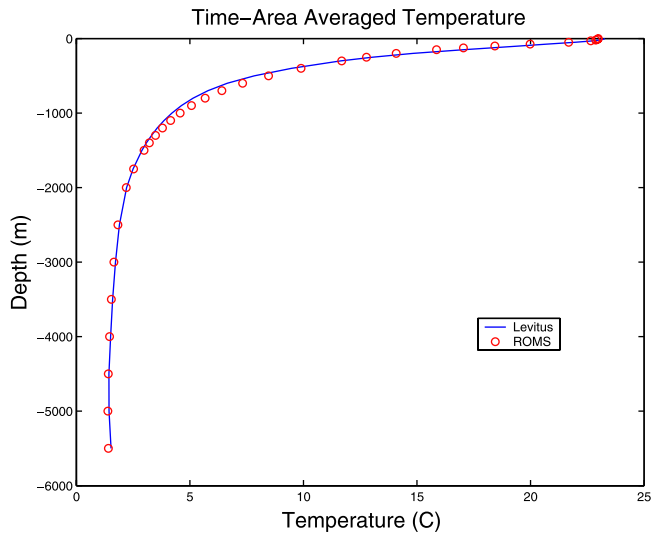

Figure 4. Time and horizontally averaged temperature profile.

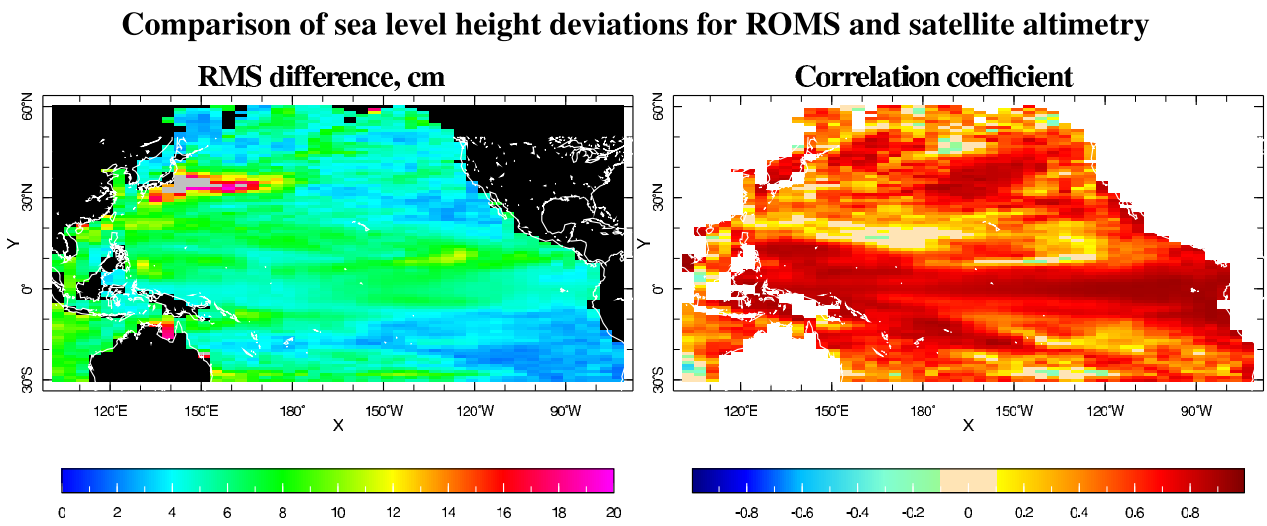

Figure 5. Comparison for 4° × 1° monthly means of the ROMS North Pacific simulation for 1996–2002 forced by daily fluxes from the NCEP-NCAR Reanalysis [*Kalnay et al.*, 1996] with sea level heights from SSALTO/DUACS time-delayed merged altimetry maps.

of 0.001 psu per year. To understand where the warming trend has the largest effect, we plot a horizontally and temporally averaged temperature profile, at the Levitus standard depths ($\overline{T}^{xyt}$). As seen in Figure 4, the most noticeable drift is at the mid-depths of 500–1500 m. The cause for the mid-depth drift is likely to be excessive mixing. This can be either on a basin-wide scale or more localized in some of the marginal seas (e.g., the Sea of Okhotsk and the Bering Sea), where the lack of a sea ice model will lead to anomalous water mass formations. The adjustment timescale for the deep ocean is longer than the duration of this simulation and we do not, as expected, see any significant changes in the deep ocean tracer fields. It should be noted that the drift shown in Figure 4 is an integrated response to the sequence of spin-up and hindcast simulations. Even if the departure from climatology during the hindcast simulation is purely due to model inaccuracies, the overall drift is not deemed to be a significant source of error for the current work since it is several orders of magnitude smaller than the signals we are analyzing.

4. Performance of the Hindcast Simulations

[23] In order to evaluate the basin-wide skill of the hindcast simulations H-N and H-Q, we compare the model output with the sea surface height fields from the SSALTO/DUACS delayed time product distributed by AVISO at ftp://ftp.cls.fr/pub/oceano/enact/msla/merged. This product uses the *Ducet et al.* [2000] approach to combine TOPEX/Poseidon, ERS-1,2, and Jason altimetry data into weekly global sea surface height anomaly maps with the spatial resolution of $\frac{1}{3}°$. Following *Kaplan et al.* [2004], the comparison is performed using 4° longitude × 1° latitude resolution. Figure 5 shows the root-mean-square (RMS) and correlation coefficient for the model and data sea surface height time series during the 1996–2002 period. This comparison highlights the model ability to reproduce large-scale features of the ocean circulation in the North Pacific. The analysis shows positive correlations in most regions; in the tropical and Eastern Pacific positive correlations can be higher than 0.8. The RMS difference is below 4 cm in many areas with the errors generally smallest in the Eastern Pacific. The poorest correlation and largest RMS differences occur in the western Pacific where the model is unable to reproduce the observed monthly variability. We conclude that in this region the dominant mode of monthly variability is related to the western boundary current and its associated dynamics (e.g., meanders, eddy formation) which at the current spatial resolution of 0.4° the model is unable to reproduce. Another region where the correlation deteriorates is in the eastern and northern Gulf of Alaska and along the southern side of the Aleutian islands. These are regions where long-lived (several years) anticyclonic eddies, denoted as Haida, Sitka, and Yakutat eddies, have been observed [*Crawford et al.*, 2000; *Ladd et al.*, 2005], but are poorly represented by the model at the current resolution.

[24] While many features of the North Pacific circulation and its variability are reproduced by the model, the comparisons shown in Figure 5 also indicate deficiencies in the numerical solution. We make the observation that the patterns of error seen in Figure 5 reflect features of the oceanic circulation (most obviously western intensification). We speculate that inaccurate representation of subgrid-scale processes (below 0.4° in this case) is the main contribution to the errors in the large-scale mean circulation. However, we cannot discount at this stage that errors in the forcing fields can also result in dynamical looking errors in model response. A more complete analysis of the sources of model error is beyond the scope of this paper.

[25] *Kaplan et al.* [2004] use the concepts of small-scale and short-term variability as useful measures of model performance. In their paper, small-scale spatial variability is estimated by the RMS deviation of a property (SSH in this case) from its space-time mean inside a 4° × 1° × 1 month bin $\left(\sqrt{\left[\sigma^2_{4°\times1°}(SSH)\right]_{1\text{month}}}\right)$; short-term temporal variability is represented as the intra-month variance of spatial means averaged over all available time periods in the given spatial bins ($\sigma_{1\text{month}}([SSH]_{4°\times1°})$). In the above

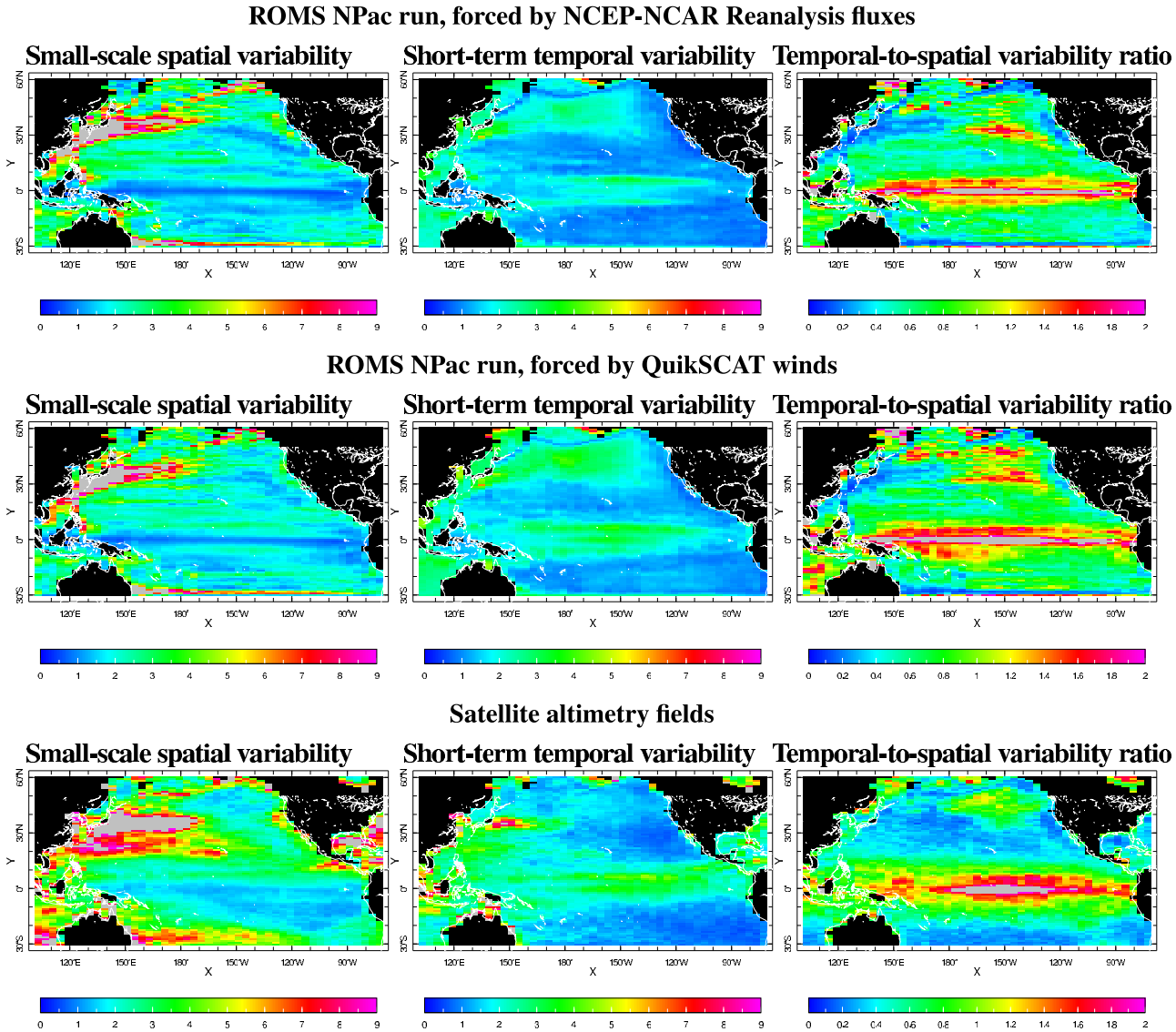

Figure 6. Comparison for 4° × 1° monthly means of the ROMS North Pacific simulation for 2000–2002 forced by either daily fluxes from the NCEP-NCAR Reanalysis [*Kalnay et al.*, 1996] or QuikSCAT winds with sea level heights from SSALTO/DUACS time-delayed merged altimetry maps.

definitions, σ is the standard deviation, and brackets represent a mean. These statistics are averaged with a square over all available months in the 2000–2002 (QuikSCAT simulation) period. Model fields are taken with three-day temporal resolution and the altimetry maps with their 7-day resolution.

[26] Figure 6 presents estimates of small-scale and short-term types of variability obtained from model simulations H-N, H-Q and from the altimetry data. The model (with 0.4° resolution) spatial and temporal variabilities are typically lower than the values obtained from satellite observations. In a few regions, such as the central North Pacific, the model and satellite-derived variabilities are of similar magnitude. In general, the model underestimates the spatial variability more than it underestimates the temporal variability. The ratio of temporal to spatial variability which to a large extent is controlled by dispersion relationships for planetary waves [*Kaplan et al.*, 2004], and thus shows a strong latitudinal dependence, tends to be higher in the model when compared to altimetry-based estimates, especially to the north of 20°N.

[27] The lack of small-scale variability in model simulations of the ocean is sometimes attributed to insufficient variability detail in the atmospheric forcing data sets. In our North Pacific simulations, however, the use of NCEP-NCAR Reanalysis and QuikSCAT winds produced similar small-scale spatial variability. One noticeable exception are the upwelling regions (along the coast of North America during the summer months, for example) where the distribution of variability was more realistic. This result agrees with *Milliff et al.* [1999], who concluded that differences in the mean wind, and not in the mesoscale variability in the wind, impact the response of a much coarser (than 0.4°) resolution ocean circulation model. In fact, the temporal variability was more strongly affected by the QuickSCAT winds resulting in an even higher time-to-space variability

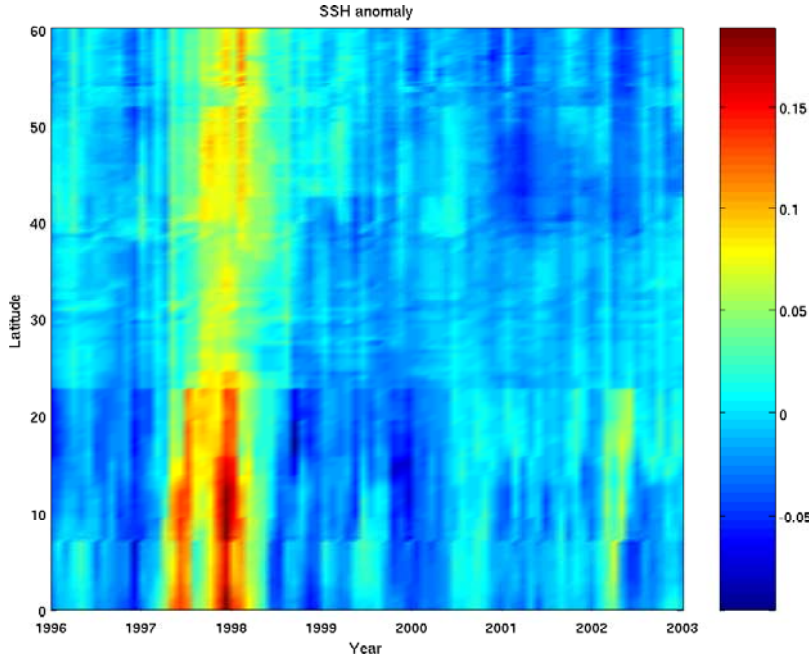

Figure 7. Time versus distance plot of sea surface height anomalies (centimeters) along the coast of North America.

ratio when compared to the Reanalysis-forced run (Figure 6).

5. The 1997/1998 El Niño

[28] We proceed by evaluating model performance in reproducing large-scale events that had observed impacts on ecosystems in the northeast Pacific in the late 1990s. The dominant mode of observed interannual variability in the equatorial and eastern Pacific is related to the El Niño/La Niña cycle. Figure 7 shows a latitude versus time plot of the sea surface height anomaly along a transect beginning in the eastern equatorial Pacific and extending along the coast of North America to the Gulf of Alaska. The anomalies are derived relative to a monthly climatology of the computed sea surface height.

[29] The 1997/1998 El Niño is characterized by a signal with an amplitude which can be three times bigger than that of the seasonal cycle. Sea surface height anomalies greater than 15 cm are seen in the early part of 1998 whereas typical seasonal variations during the period of this simulation are less than 5 cm. The initial coherent pulse of the El Niño emerges in the eastern equatorial Pacific during the spring of 1997 and lasts through the summer. A second pulse is observed in late 1997 and lasts through the early months of 1998. The overall duration of each distinct pulse is similar (approximately 4 months) though the second fall/winter pulse has significantly larger anomalies. Both the spring/summer and fall/winter pulses appear to stall at around 23°N (Baja California Peninsula). A weak but distinct signal is seen in the midlatitudes with a slight intensification north of 40°N. This pattern of anomalies (strong near the equator, weak in middle, and strong in high latitudes) is suggestive of an oceanic response primarily to atmospheric teleconnections in the high latitudes and not to changes propagated by the coastal wave guide. It is noteworthy that the smoothed bathymetry in the current implementation implies reduced scattering of shelf-waves and may result in a more transmissive waveguide than is expected. In the context of the current suite of simulations, the atmospheric versus oceanic forcing problem is further explored by A. J. Hermann et al. (A comparison of remote versus local influence of El Niño on the coastal circulation of the northeast Pacific, manuscript in preparation, 2005) (hereinafter referred to as Hermann et al., manuscript in preparation, 2005), who show that most of the El Niño-related variability in the Gulf of Alaska can be explained while omitting contributions of remote (equatorial) oceanic

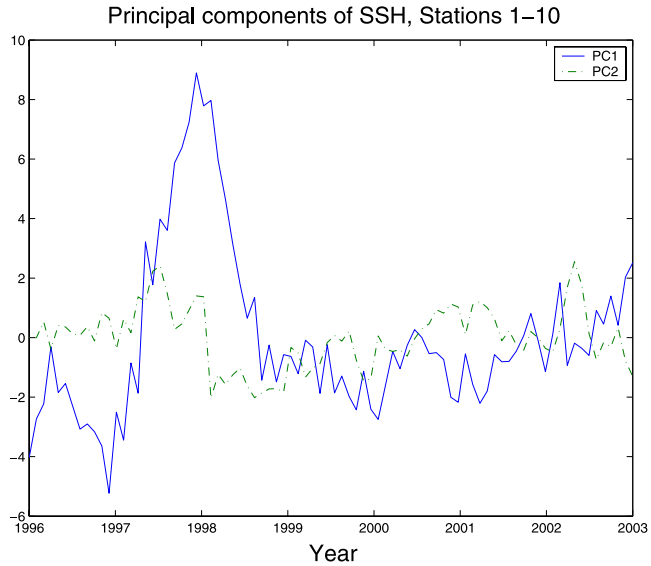

Figure 8. First two principal components of SSH anomaly time series corresponding to Figure 7.

Table 1. Correlation Coefficients of Sea Surface Height Anomalies Between Station 1 (Latitude 9.3°N) and Station N Along the Coast of North America

Station Number	Location	Latitude (North) of Station	Correlation Coefficient (r)
3	southern Mexico	21.1	0.83
4	Baja California	27.9	0.77
6	California	46.7	0.69
10	Alaska	58.9	0.67

origins. A principal component analysis of the anomaly data (Figure 8) shows that during the period of this simulation (1990–2003) the El Niño signal is the dominant mode of variability along the coast of North America. The two leading principal components represent 79% and 10% of the variability, respectively.

[30] Cross-correlation coefficients of sea surface height anomalies between a station near the equator (station 1 at 9.3°N, off the coast of Panama) and various stations along the coast of North America are presented in Table 1. The correlation coefficient for the stations within the region of maximum El Niño influence (south of 23°N) are 0.77 to 0.83 which correspond to the values (0.75 to 0.84) derived from the altimetry analysis of *Strub and James* [2002]. Our correlation value between the equator and Alaska of 0.67 is considerably higher than the 0.41 of the satellite derived product. This is likely due to the inadequate representation in the model of the steep and narrow shelf off the coast of North America which limits the effectiveness of shelf-wave scattering.

[31] We look at the effect of El Niño on the water mass properties and circulation in the California Current system. We choose a transect at 44°N off the coast of Oregon which is sampled as part of the GLOBEC Northeast Pacific program. Figure 9 shows the January/February 1998 temperature anomaly relative to 1997, a non-El Niño year, for up to 250 km offshore. The figure shows the upper 400 m, which encompasses the euphotic zone and the source region for the summer upwelled waters in this region (in addition to exhibiting the most significant response to the event). During the height of the 1997/1998 El Niño, the model shows that temperatures in the upper water column in the California Current were 1°C higher than those in a non-El Niño year. The largest temperature anomalies are seen at about 100 to 150 m depth owing to the deeper (winter) thermocline corresponding to the positive sea surface height anomaly of the El Niño signal.

[32] We also point to the sharp tilt of the anomalous isotherms near the coast. An anomalous northward current with velocities that reach more than 50 cm/s (figure not shown) is seen during the El Niño event. Thus the overall picture during a strong El Niño event, such as during 1997/1998, is of an increased sea level height near the coast accompanied by an anomalous northward current and higher temperatures in the upper water column.

6. The 1999 North Pacific "Regime Shift"

[33] A change in the state of the North Pacific, sometimes referred to as a "climate regime shift," was observed in the period of 1999–2002 [*Bond et al.*, 2003; *Peterson and Schwing*, 2003]. Following the analysis of *Bond et al.* [2003], we plot the sea surface temperature anomaly (SSTA) for the winters (November–March) of 1999–2002 relative to all available winters and compare it with a similar plot from the data of *Rayner et al.* [2003] (Figure 10). The new state of the North Pacific is characterized by a prominent midlatitude warming in the western part of the basin with a tongue extending to 200°E, and a cooling along the whole eastern part of the basin, extending west across the basin to the Sea of Okhotsk north of about

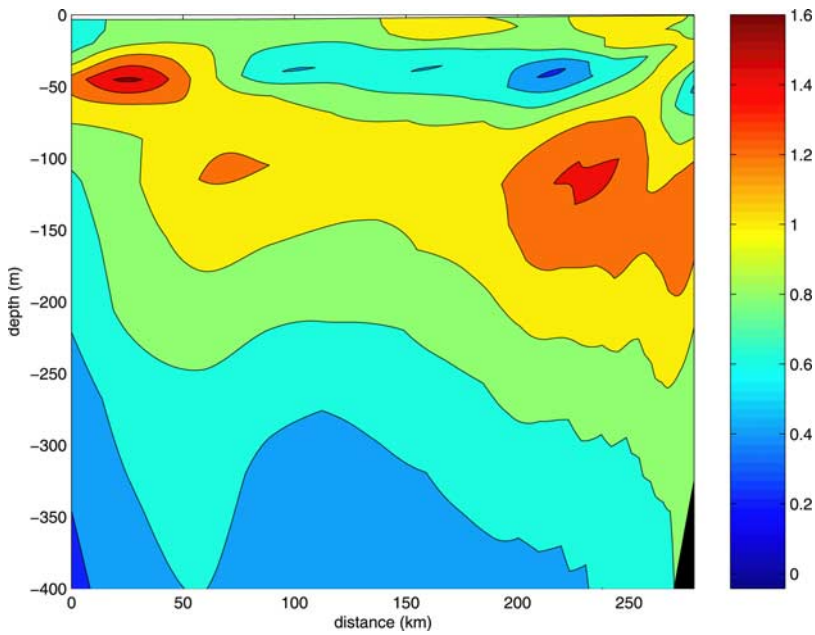

Figure 9. Temperature anomaly of January/February 1998 relative to 1997. The transect is at 44°N, with the offshore end at km 0.

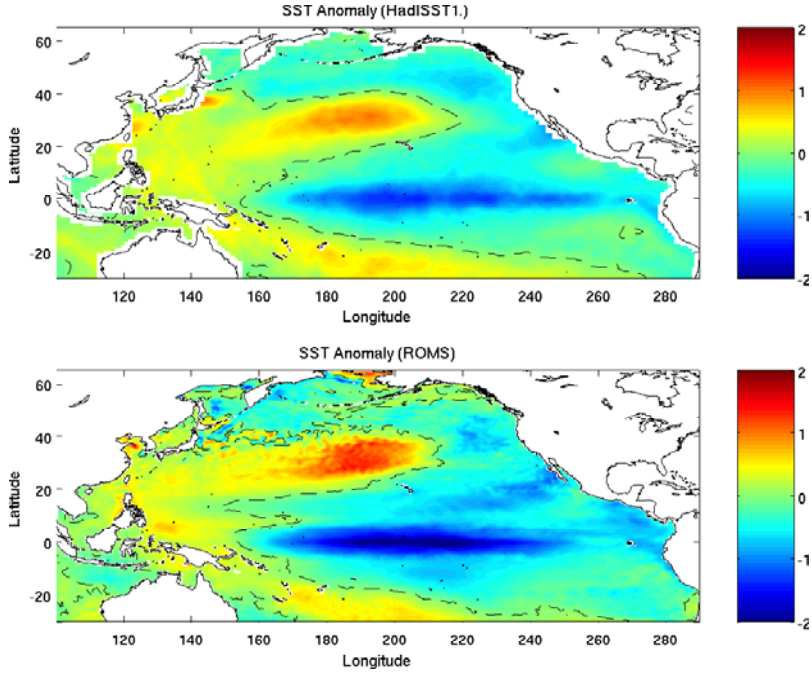

Figure 10. Data and model sea surface temperature anomalies for the winters (November–March) of 1999–2002.

40°. In the northeast Pacific, the temperature anomalies can reach 1°C. Figure 10 shows both the structure and magnitude of the SSTA in the model results to be consistent with the data though the model exhibits a slightly larger amplitude in the SSTA. The first principal component of the SSTA (not shown here) correlates with the PDO index. Figure 11 shows the evolution of the second principal component, with a clear change of state in 1998. The corresponding empirical orthogonal function (EOF) shows the pattern of the SSTA in Figure 10. The analysis of the model results mirrors the conclusions reached by *Bond et al.* [2003], in that the change in state of the North Pacific in the late 1990s cannot be exclusively explained by the PDO index. The simulated change of state and the corresponding principal component analysis both demonstrate the model's ability to represent observed interannual variability of large-scale phenomena in the North Pacific.

7. The 2002 Northeast Pacific Cold Anomaly

[34] The "cold anomaly" in the northeast Pacific in 2002 refers to observed subsurface upper ocean waters off the coasts of Oregon and Vancouver Island which were more than 1°C cooler and 0.4 psu fresher than in 2001 (see Figure 12 reproduced from *Freeland et al.* [2003]). The presence of the cold anomaly in the upwelling waters off the coast of Oregon has been linked to increased biological productivity driven by a concurrent increase in the supply of nutrients to the photic zone. We examine the computed anomalies along the observational transects known as Line-P off Vancouver Island (48.5°N, 125°W to 50°N, 145°W) and Line-NH off the central coast of Oregon (150 km off shore at 44.13°N).

[35] Figure 13 shows the computed temperature anomaly from the 2002 June/July average relative to 2001 along Line P (compare with Figure 12). The effects of the anomaly are seen all the way to the coast. The model results show the core of the cooling to be between 30 and 120 m of depth with shallowing of the anomaly toward the coast. The largest anomaly is seen between 400 and 800 km shoreward of Ocean Weather Station Papa (km 0 in the plot), and with a magnitude of approximately 1.25°C. Both the magnitude and location are consistent with the observations. Both in the model and observations, the subsurface cooling is accompanied by a shallow layer of anomalous warm water of up to 1°C. The observations show the surface warming to reach up to 40 m at station P; in the model this layer is at

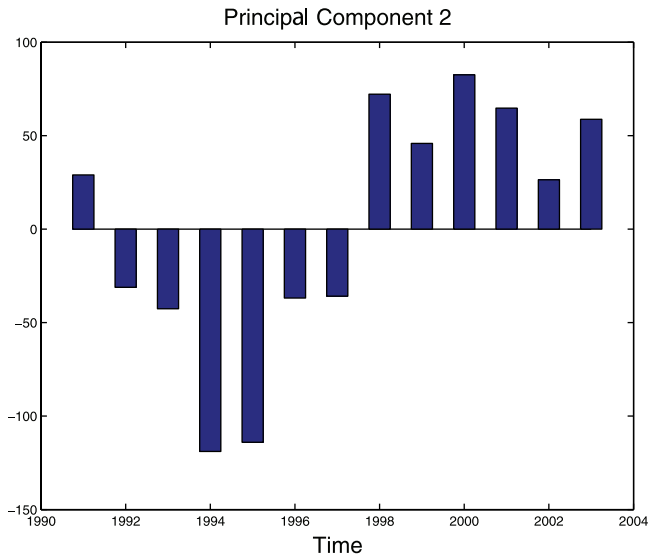

Figure 11. Second principal component of the winter sea surface temperature anomalies.

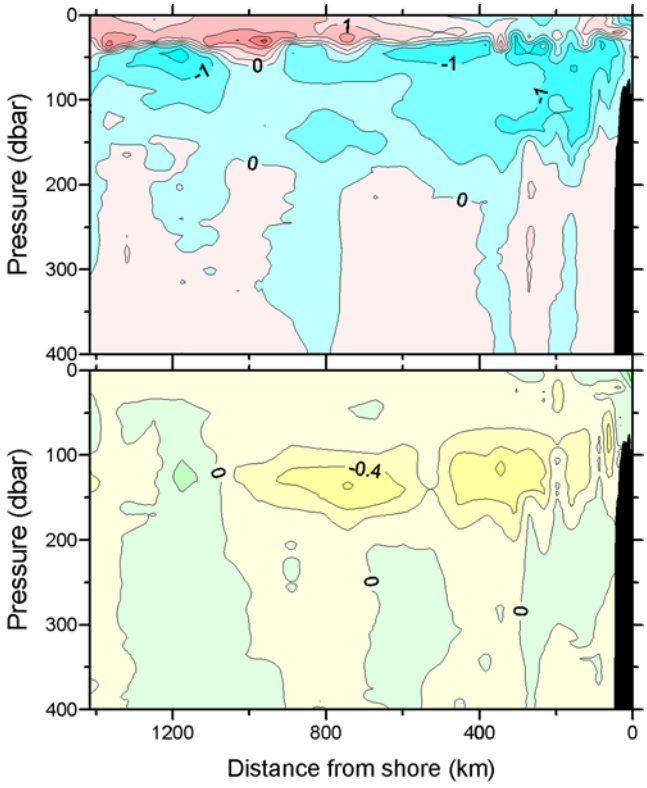

Figure 12. (top) Temperature and (bottom) salinity June/July 2002 minus 2001 anomalies along line-P. Figure reprinted with permission from *Freeland et al.* [2003].

about 25 m. This is consistent with the too-shallow mixed-layer depths observed in the model in this region. The model results (not presented here) also show a fresh anomaly of up to 0.4 psu during June/July of 2002, consistent with the observations (see bottom of Figure 12).

[36] The model results along the Newport hydrographic line (Line NH) are shown in Figure 14. Again, we show the June/July 2002 versus 2001 temperature anomaly. The anomalies along Line-NH exhibit the same offshore deepening as on Line-P, though they are generally shallower. The core of the cool water is at 20 to 50 m depth. The anomalous warm surface layer is observed here as well. A plan view of the temperature anomaly at 50 m depth covering the Gulf of Alaska and the Northern part of the California Current is shown in Figure 15. This plot shows that the anomalous cooling covered a significant portion of the Alaska gyre and extended south along the California Current.

[37] The source and cause of the observed cold anomaly are not settled issues. As noted above, *Freeland et al.* [2003] advance various, non-mutually exclusive theories for the source of the cold and fresh waters. These include enhanced winter mixing, anomalous alongshore advection, and anomalous coastal upwelling.

[38] To investigate some of these possibilities, we first look at the mean depth of the mixed layer in the winters (November–March) of 2001, 2002, and 2003 (Figures 16, 17 and 18, respectively) in the northeast sector of the model domain. The latter is to help get a sense of whether 2002 was indeed anomalous in mixing. In 2001, the mixed layer depth in the Alaska Gyre ranges from approximately 20 m to 40 m with the deeper values confined to small regions near the center of the gyre. In 2002, there is a broad area of deeper mixing in the gyre with boundary layer depths reaching 60 m. The enhanced mixing does not extend significantly to the south of the gyre. By 2003, the mean winter mixed layer depth in the Alaska Gyre is shallow again with the deeper mixing in the west and south. The strong suggestion is that in the winter of 2002 there was indeed anomalous mixing over extended areas of the Alaska Gyre.

[39] A density transect along Line-P reveals that in the model, the core of the anomalous water has a density of σ_θ =

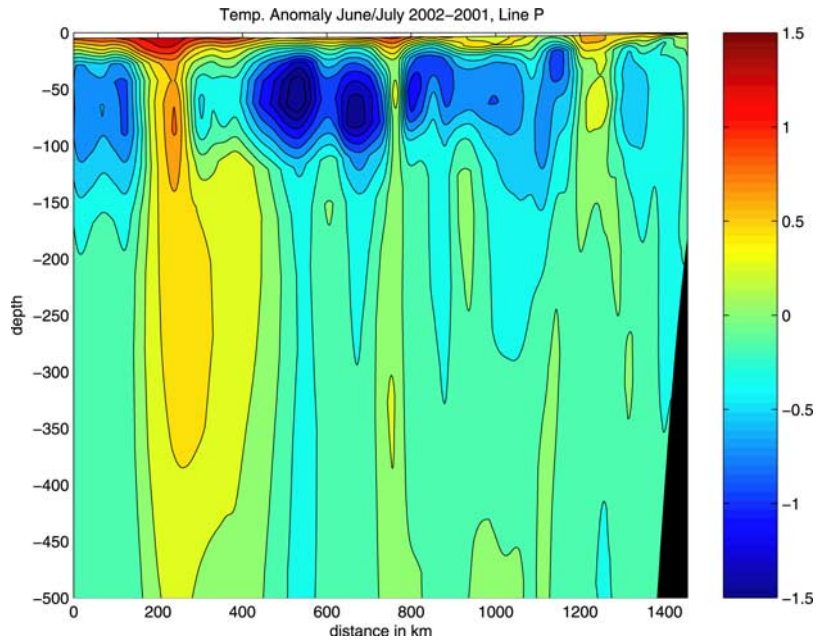

Figure 13. Temperature anomaly along Line P for June/July 2002 relative to June/July 2001.

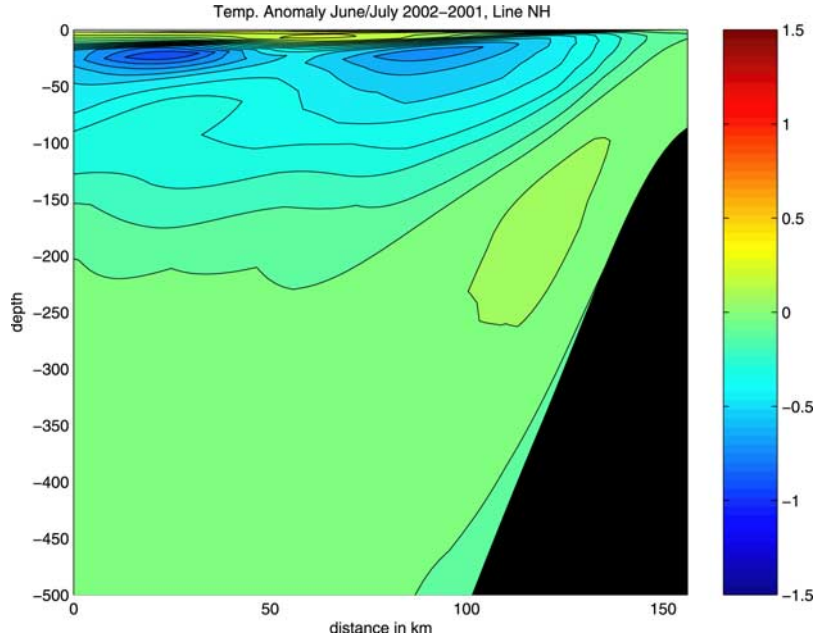

Figure 14. Temperature anomaly along the Newport hydrographic line (Line NH) for June/July 2002 relative to June/July 2001.

26.2 ($\sigma = \rho - 1000$). The depth of the 26.2 isopycnal surface is plotted in Figures 19 and 20 for the winters of 2001 and 2002, respectively. The first noticeable feature is the southern excursion of the outcropping line in the winter of 2002. This is more pronounced toward the west where the difference is a few hundreds of kilometers. The other feature is the shallowing of this layer near the coast. In the area near Line-P off Victoria Island, we notice an excursion of nearly 20 m between 2002 and 2001. An even bigger difference exists along the coasts of Washington and Oregon where a narrow tongue is nearly 30 m shallower in 2002 relative to 2001. The density maps suggest that the cold anomaly observed off Vancouver Island and the Oregon coast are the same water mass with its core lying on the $\sigma_\theta = 26.2$ isopycnal. The near-coast shallowing is also suggestive of increased upwelling/decreased downwelling in 2002.

[40] We attempt to further determine the source of the anomalous cold/fresh water by determining the path of the circulation on the $\sigma_\theta = 26.2$ isopycnal. We compute

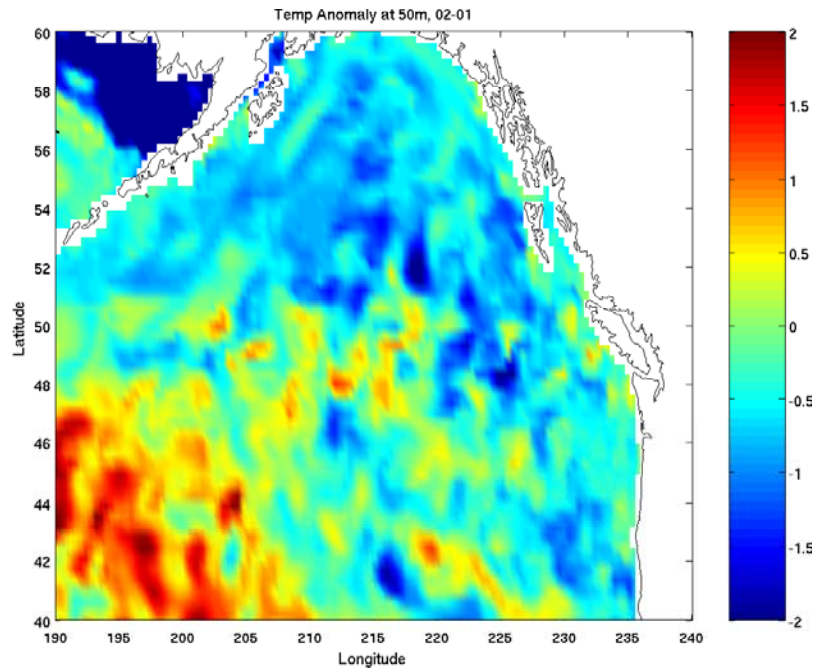

Figure 15. Temperature anomaly at 50 m for June/July 2002 relative to June/July 2001 in the northeast Pacific.

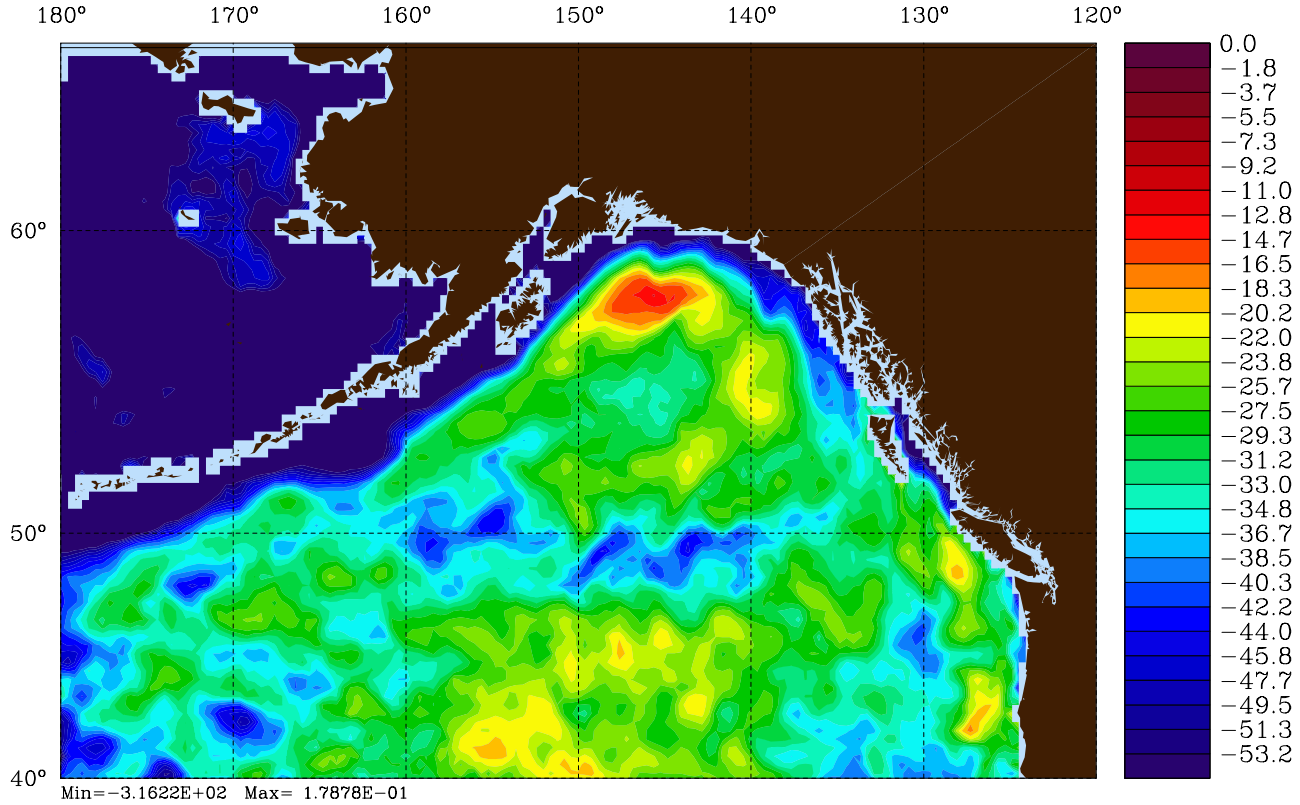

Figure 16. Mixed layer depth, winter 2001. Herein, winter is defined as November of the previous to March of the current year.

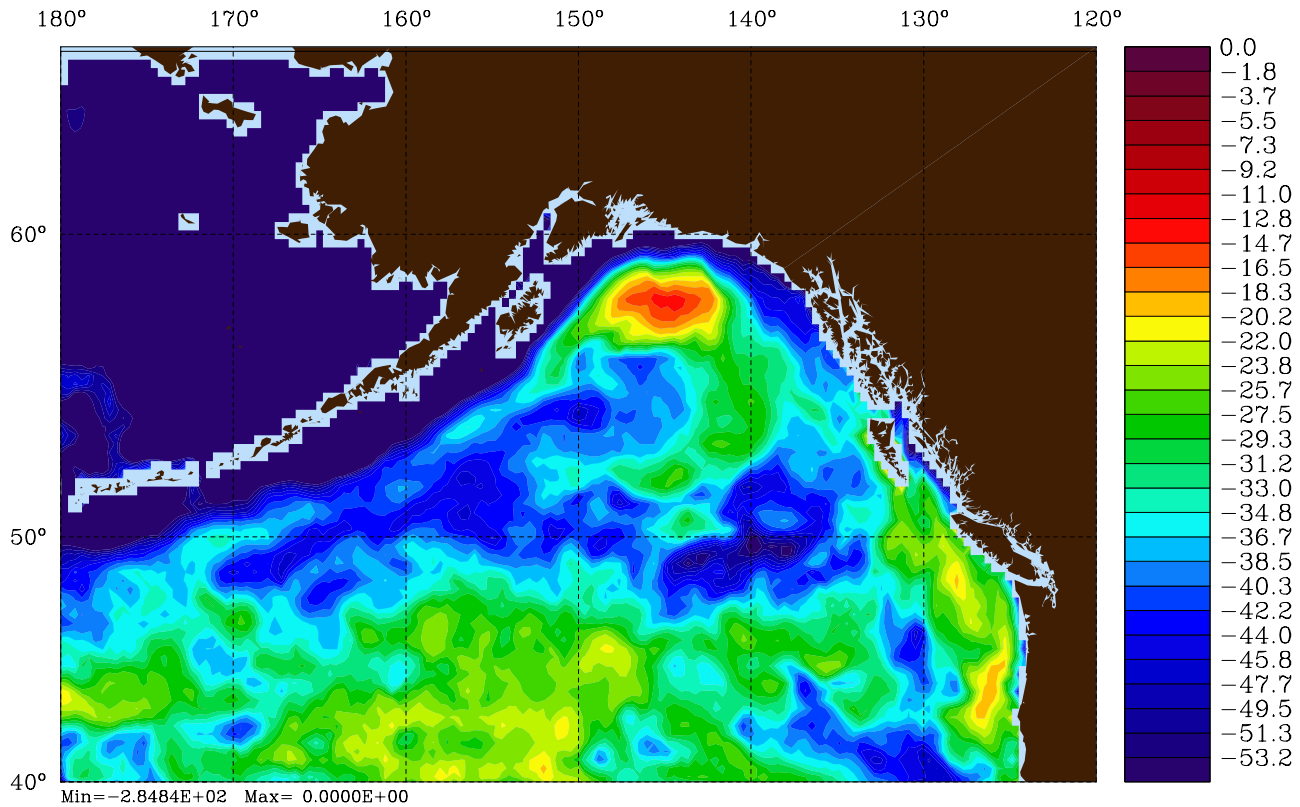

Figure 17. Mixed layer depth, winter 2002.

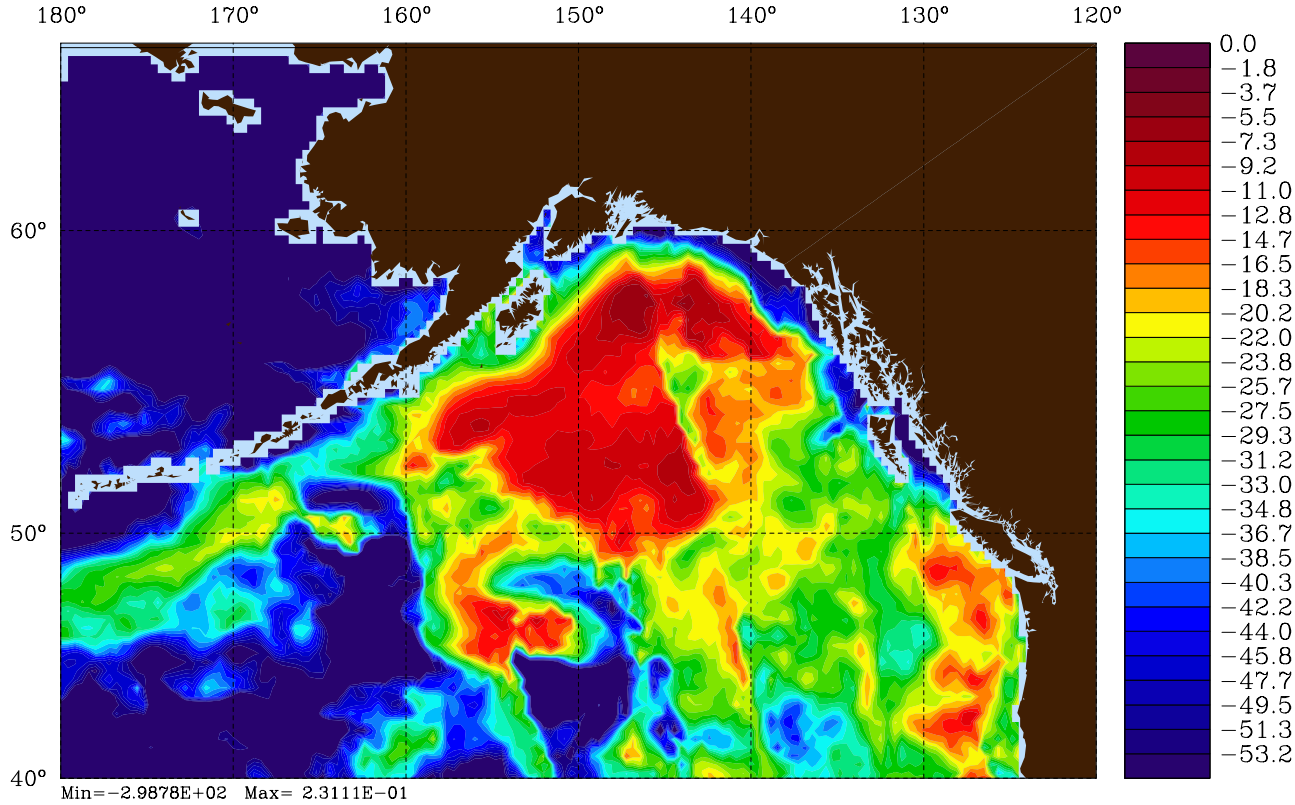

Figure 18. Mixed layer depth, winter 2003.

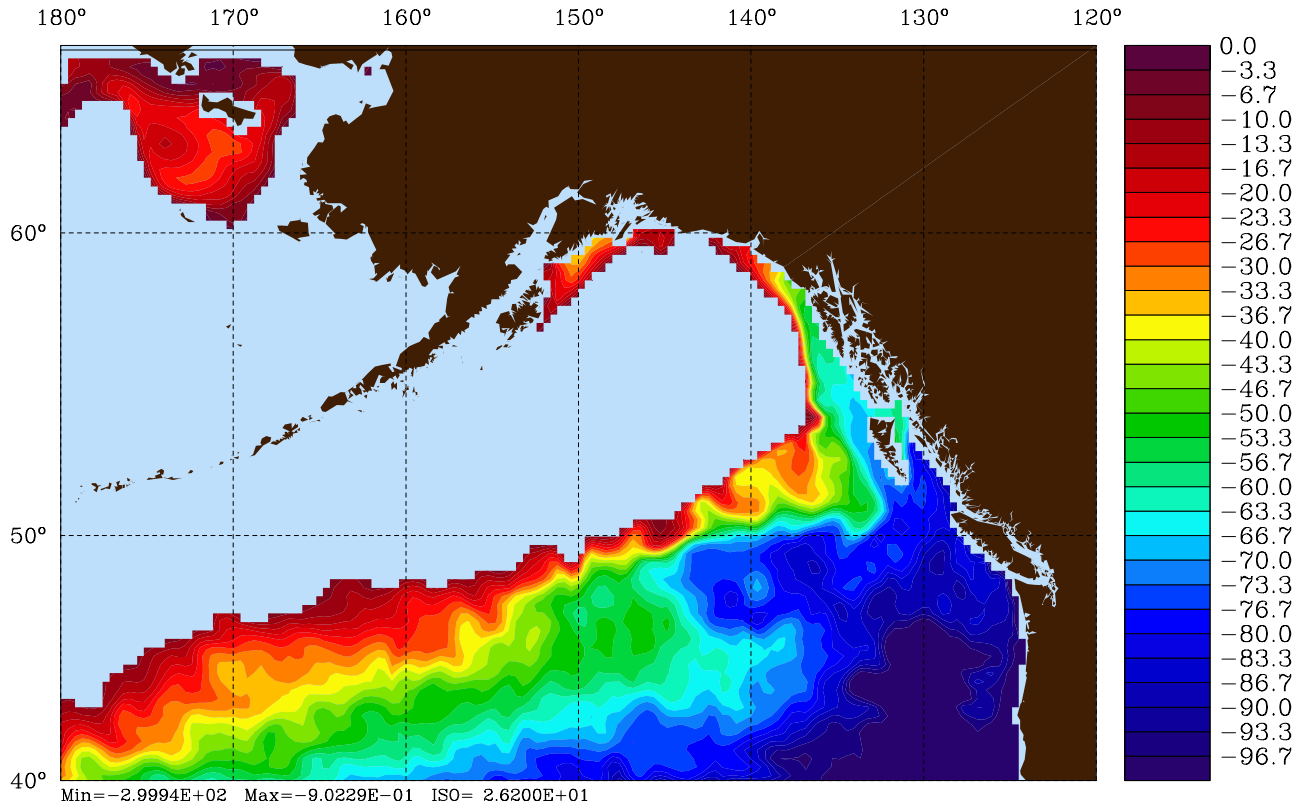

Figure 19. Depth of density surface $\sigma_\theta = 26.2$, winter 2001. Herein, the outcropping line is denoted by the juxtaposition of the color contours with pale blue shading.

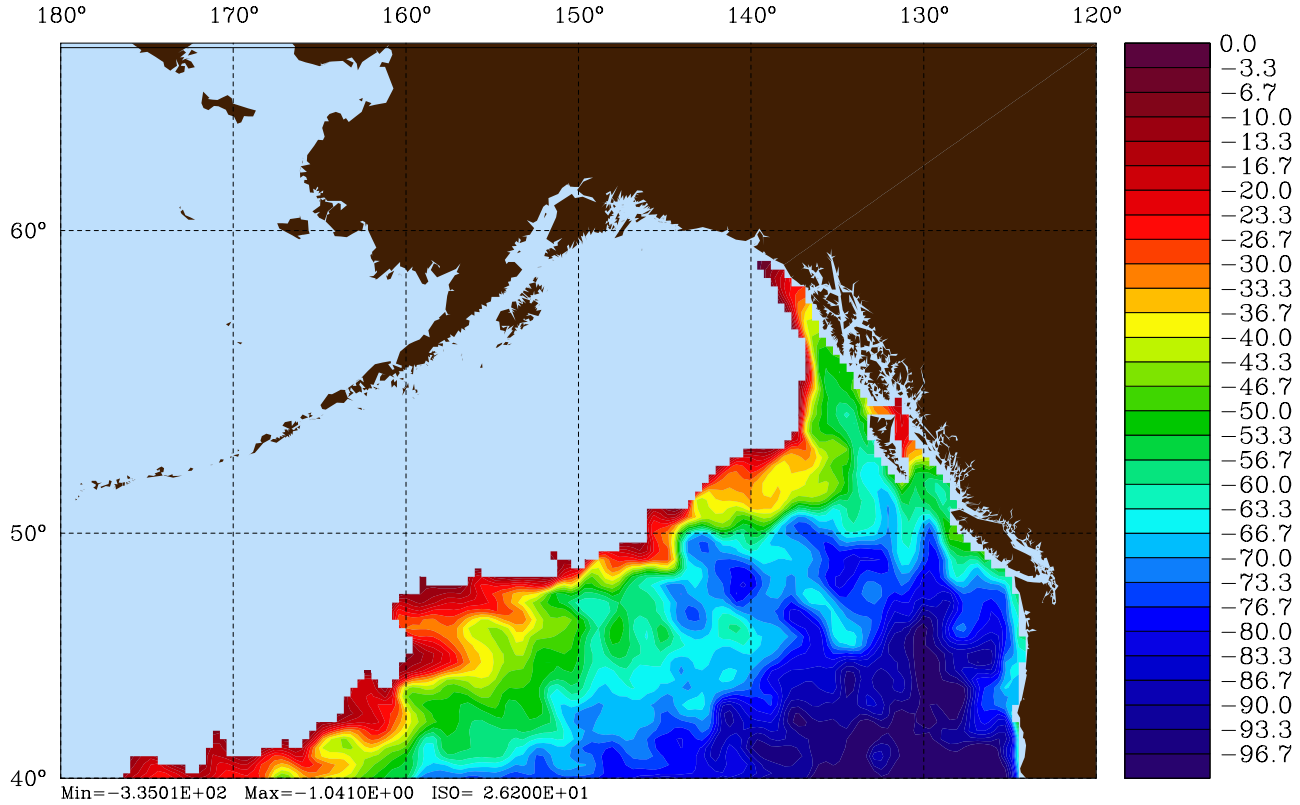

Figure 20. Depth of density surface σ_θ = 26.2, winter 2002.

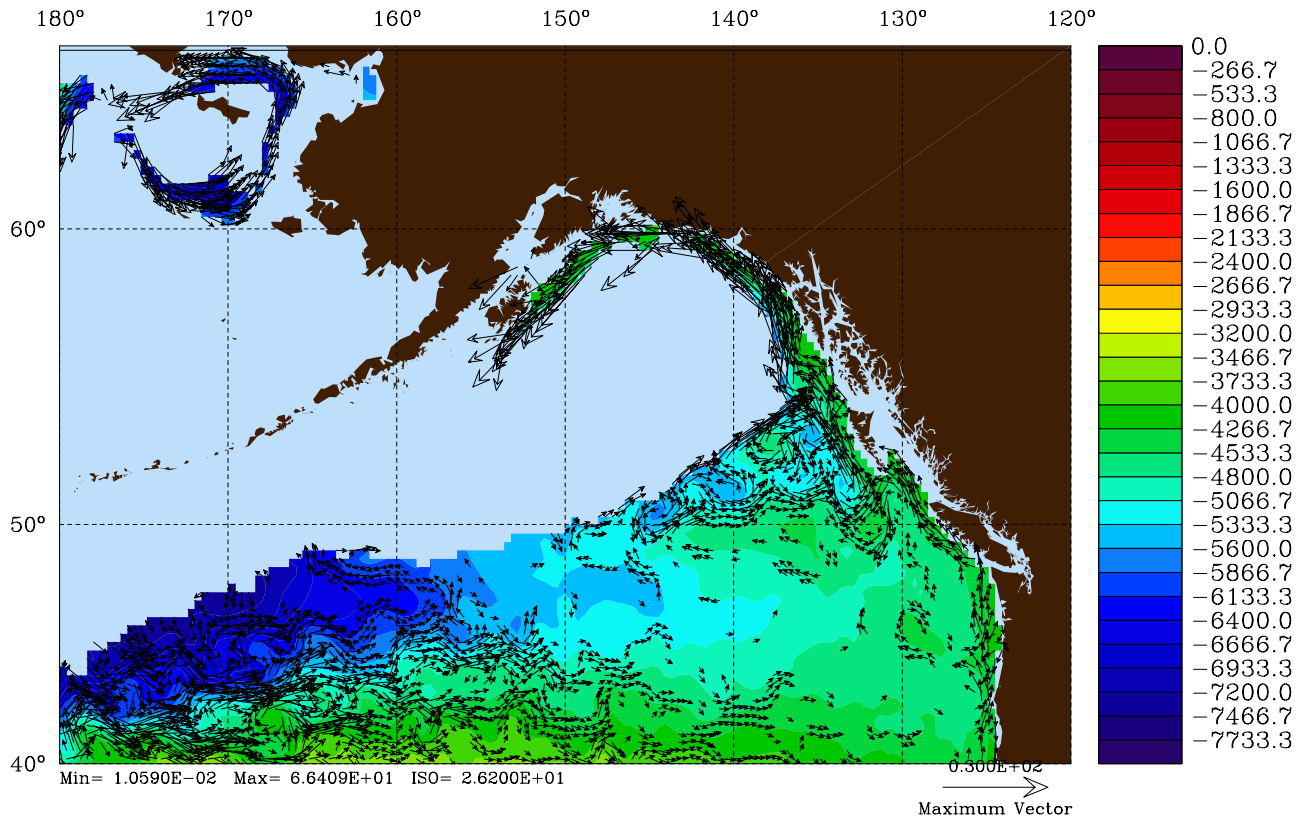

Figure 21. Bernoulli function on density surface σ_θ = 26.2, winter 2001.

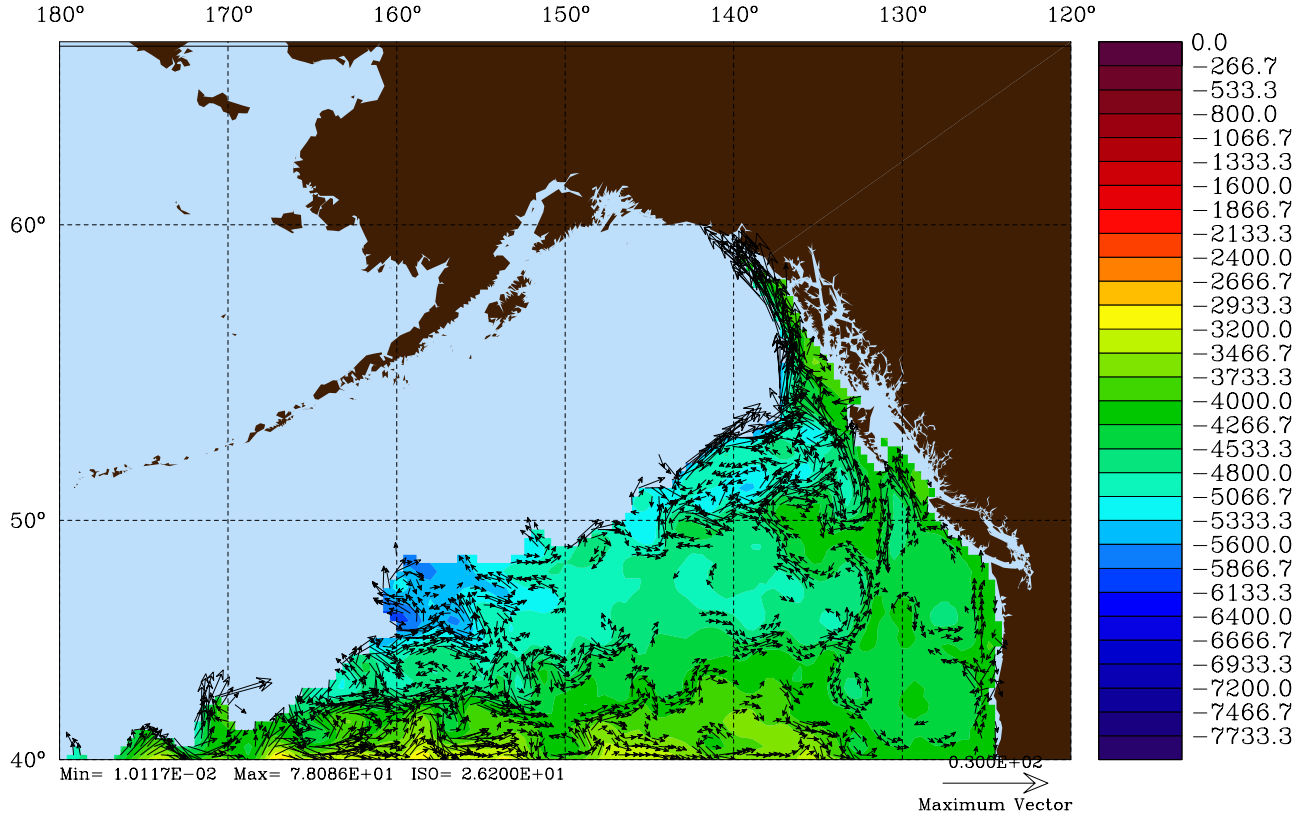

Figure 22. Bernoulli function on density surface $\sigma_\theta = 26.2$, winter 2002.

the Bernoulli function which for a stratified ocean is given as

$$B(\sigma) = \rho_o g\eta + g\int_{z(\sigma)}^{0} [\rho - \rho(\sigma)]dz, \qquad (1)$$

where $\sigma = \rho - 1000$ is a given density surface, g is gravity, and η the sea surface displacement [*Cox and Bryan*, 1984; *Malanottte-Rizzoli et al.*, 2000]. For steady inviscid flow, B-quantity is conserved following a fluid element [*Pedlosky*, 1987]. Similarly, a fluid element that moves geostrophically remains on a constant density (σ) surface. Therefore the intersection of Bernoulli and density surfaces define the streamlines for geostrophic flow in a stratified ocean. *Pedlosky* [1987] further shows that these streamlines define trajectories of conserved potential vorticity. Therefore, geostrophic circulation is parallel to Bernoulli function isolines on a given isopycnal, σ, below the mixed layer and away from both the equator and western boundary currents. Figures 21, 22, and 23 show the Bernoulli function on the $\sigma_\theta = 26.2$ isopycnal, with superimposed total velocity vectors for the winters of 2001, 2002, and 2003 respectively. In 2001 we notice that away from the line of outcropping the vectors are mostly parallel with Bernoulli isolines indicating a mostly geostrophic interior circulation. The waters off Victoria Island and the coast of Oregon are a confluence of eastward and northward currents. There is a strong eastward current along the outcropping line which becomes the Alaskan Stream. In the winter of 2002, the patterns are distinctly different. The most obvious change is the much weaker northward current along the coast implying an anomalous southward flow in 2002. We also notice the more ageostrophic flow, which can be recognized as velocity vectors not parallel to Bernoulli isolines, in the western part of the domain indicating a broader spatial scale for the ventilation of the water on this isopycnal. Furthermore, in 2002, there is a decrease in the gradient of the Bernoulli function between the outcropping line and the regions where the cold anomaly was observed. The homogenization in the Bernoulli quantity creates a pathway through which water can flow between the ventilated and the anomalous region geostrophically. This is accompanied by a marked decrease in the eastward transport of the surface current along the outcropping line. In 2003, we see a situation that more closely resembles 2001 with a significant along-shore current and an increased gradient of the Bernoulli function between the coasts of Oregon/Vancouver Island and the outcropping line of the isopycnal.

8. Discussion and Concluding Remarks

[41] A numerical simulation of the circulation in the North Pacific basin for the period of the late 1990s and early 2000s is shown to represent observed large-scale variability with significant skill. A comparison with the time-delayed, merged satellite altimetry product from SSALTO/DUACS shows high correlations in the tropics and eastern Pacific, and lesser agreement in the west where the model resolution (0.4°) is inadequate for resolving the dynamics associated with the western boundary current. Use of the high-resolution, scatterometer-derived wind product is shown to increase temporal, but not spatial, variability in

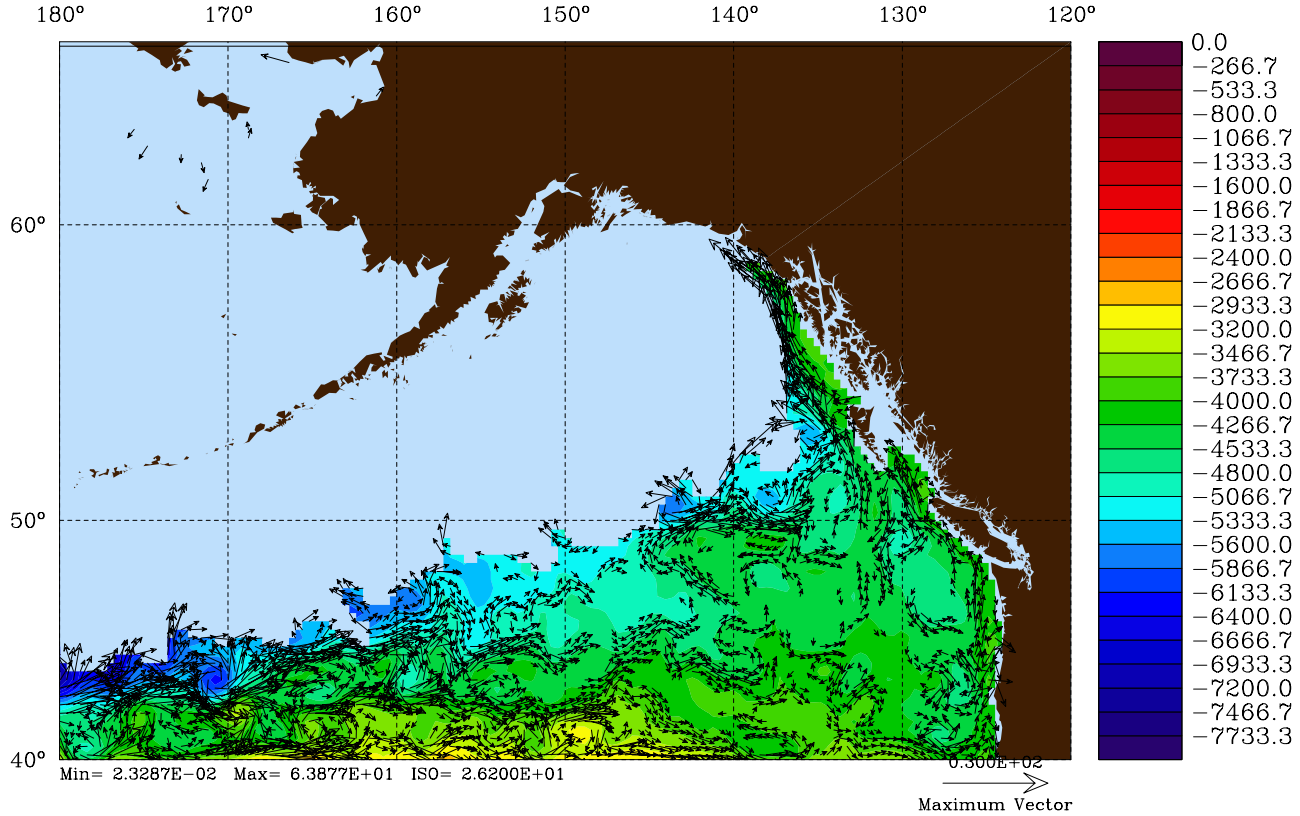

Figure 23. Bernoulli function on density surface $\sigma_\theta = 26.2$, winter 2003.

the model. Nevertheless, the better mean winds of the scatterometer do improve particular ocean circulation features such as upwelling both in the equatorial and the eastern Pacific. A more detailed description of the effects of using satellite-derived winds is beyond the scope of this paper and will be addressed in a separate publication.

[42] Model drift from climatology over the 2 decades of simulation (spin-up plus hindcast) was shown to be several orders of magnitude smaller than the variability of the phenomena investigated here. This is a necessary condition for any successful study of climate-scale variability in the ocean. This result is consistent with other implementations of ROMS for basin-scale computations [e.g., *Haidvogel et al.*, 2000]. Furthermore, it validates the model as a potential tool for studying interdecadal variability in ocean conditions.

[43] Three large-scale modes of variability are investigated: (1) the 1999 North Pacific regime shift, (2) the 1997/1998 El Niño, and (3) the 2002 subsurface cold anomaly in the northeastern Pacific. These phenomena were chosen for three principal reasons. First, they test different aspects of model performance such as the ability to reproduce interdecadal and interannual variability, surface and subsurface as well as basin- and regional-scale oceanic response. Second, the occurrence of these events have been linked to changes in faunal community composition and abundance in the northeast Pacific, the focus region for GLOBEC-NEP and finally, these events are concurrent with the extensive GLOBEC-NEP field program.

[44] Sea level pressure and sea surface temperatures in the North Pacific after 1999 are in a state reminiscent of the pre-1976 conditions indicating a possible regime shift back to a relatively cool northeast, and warm southwest, Pacific [*Bond et al.*, 2003]. Whether this pattern holds remains to be seen. Nevertheless, there has been an increase in the observed biomass in the northeast Pacific (including salmon populations which is a GLOBEC target species) following the new physical state since 1999. An analysis of the model output is consistent with the results of *Bond et al.* [2003] suggesting that this shift is not explained by the leading mode of variability which is represented by the Pacific Decadal Oscillation. Even though there is a significant separation in the percent of the variability explained by the two leading principal components, the biological observations show correlations with both modes [*Bond et al.*, 2003; *Hare and Francis*, 1995; *Mantua et al.*, 1997]. The model representation of this broad signal is a measure of its ability to generate the correct interannual variability. A study of the particular adjustments in the physical characteristics of the various subregions in the Pacific to this basin-scale change of state is beyond the scope of this paper. As discussed in section 1, observational evidence hints at a non-uniform response in the northeast Pacific both in the physical and ecosystem characteristics providing motivation for further exploration.

[45] As presented in several observational studies [*Dever and Winant*, 2002; *Kosro*, 2002; *Strub and James*, 2002], the model results show that the 1997/1998 El Niño produces changes in the circulation along the coast of North America from the equator to the northern Gulf of Alaska. The most pronounced effects are seen between the equator and about 23°N (Baja California) where the coastal regions are pre-

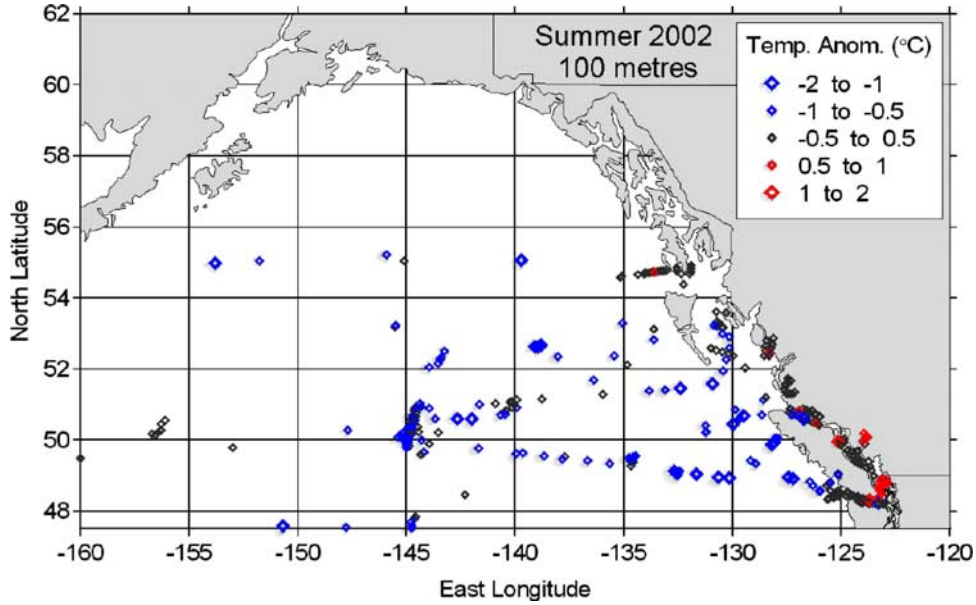

Figure 24. Temperature anomaly at 100 m for summer 2002 showing the broad extent of the anomalous event. Data are a blend of XBT, CTD, and Argo floats. Reprinted with permission from *Crawford et al.* [2005].

dominantly forced by oceanic waves originating in the equator. The coastal trapped wave is seen to propagate farther north to the Gulf of Alaska, though its signal is considerably weaker north of 23°N. Though there are significant correlations between the equatorial and the Gulf of Alaska coastal regions during the El Niño event, indications are that atmospheric teleconnections contribute the major source of local variability in the northern latitudes. One of the more noticeable dynamical changes during the El Niño period is the increased sea level height along the whole coast of North America. Anomalies can reach 20 cm particularly in the subtropics. The increase in sea level is accompanied by a depression of the thermocline and an increase in the heat content of the upper ocean in the coastal region. The model results also show an anomalous northward current along the coast. Therefore the increase upper ocean heat content is a result of both a deeper thermocline and a decrease of southward advection of cold subarctic waters. The principal component analysis shows that during the event, El Niño is the dominant mode of variability in the coastal regions of North America.

[46] The circulation model shows that the anomalous cold event observed at various stations in the northeast Pacific in 2002 was a large-scale event covering the Gulf of Alaska and extending south along the coasts of Washington and Oregon (Figure 15). This result is consistent with the observations presented by *Crawford et al.* [2005] based on a blend of XBT, CTD and Argo float data (see Figure 24). Measured (and modeled) temperature anomalies reached more than 1°C colder and salinities 0.4 psu fresher than the previous year at depths ranging from 30 to 150 m. This event was accompanied by a warmer than usual surface layer.

[47] From the model, we ascertain that the event was a result of enhanced winter mixing in the center of the Alaska gyre just prior to the anomalous measurements in the summer of 2002. This was accompanied by a shallowing of the σ_θ = 26.2 isopycnal and a homogenization of the Bernoulli function on this isopycnal, which resulted in water being advected from the center of the Alaska gyre to the coastal regions off Vancouver Island and the coasts of Washington and Oregon. Enhanced surface heat fluxes in the summer created a warmer than usual surface layer which capped the anomalous cold and fresh water in a stable water column. Since the anomalous cold waters are below the typical mixed layer in this region, we anticipate that the cold/fresh anomaly will persist until either another anomalous mixing event or slow dissipation takes place.

[48] The North Pacific domain (NPac) is the largest scale of the suite of models that we have developed to address the issues pertinent to the GLOBEC program in the northeast Pacific. With the explicit goal of assessing the model ability to reproduce the main circulation features and the climate-scale variability in this domain, we have evaluated the general model skill and investigated three large-scale events with observed influence in our region of interest. The current setup of the model (ROMS) for this domain emerges as a credible tool for this work. Model drift over multi-decadal integration periods is below the levels of variability of the events of interest. Furthermore, the model is able to generate observed modes of variability in a range of spatial and temporal scales and in a variety of dynamical regimes (e.g., equatorial, midlatitude and subpolar regions). These are the necessary conditions for further work in the high-resolution local domains which rely on NPac to generate the climate-scale variabilities which are then linked to changes in the regional ecosystems. We have successfully used output from NPac in the high-resolution physical and coupled biophysical regional models [e.g., *Powell et al.*, 2005; Hermann et al., manuscript in preparation, 2005].

[49] Although the NPac model is too coarse in its spatial resolution to be able to resolve some of the details (e.g.,

mesoscale eddy transports, topographic features, etcetera), it can nevertheless be used to address some of the questions of interest to the GLOBEC program beyond simply providing initial and boundary conditions to the high-resolution regional domains. In particular, we were able to study how large-scale variability affects the local circulation in both the Gulf of Alaska and the northern reaches of the California Coastal Current and investigate questions regarding origins of anomalous water masses which cannot be effectively modeled in regional settings.

[50] **Acknowledgments.** The authors would like to thank Bill Crawford from the Institute for Ocean Sciences (IOS) in Sidney, BC, for providing a figure and for significant discussion relating to topics in this paper, as well as the reviewers for their insightful comments. We further acknowledge Howard Freeland (IOS) for providing a figure used in our comparisons. The altimeter products were produced by the CLS Space Oceanography Division as part of the Environment and Climate EU ENACT project (EVK2-CT2001-00117) and with support from CNES. Other data were obtained from the U.S. GLOBEC northeast Pacific website (http://globec.coas.oregonstate.edu/groups/nep/index.html). Main funding for this work was provided by National Science Foundation grants OCE00-02892 and OCE01-13461. This publication was also partially funded by the Joint Institute for the Study of the Atmosphere and Ocean (JISAO) under NOAA Cooperative Agreement NA17RJ1232. Alexey Kaplan was funded by NOAA JCSDA grant NA03NES4400012. The QuikSCAT data was provided by Xiajun Yuan from LDEO and funded by NASA grant JPLCIT-1216483. Acknowledgment is made to the National Center for Atmospheric Research, which is sponsored by the National Science Foundation, for computing time used in this research. This publication has U.S. GLOBEC contribution 256, LDEO contribution 6793, JISAO contribution 1140, NOAA Pacific Marine Environmental Laboratory contribution 2815, and Fisheries-Oceanography Coordinated Investigations contribution FOCI-G555.

References

Batchelder, H., and T. Powell (2002), Physical and biological conditions and processes in the northeast Pacific Ocean, *Prog. Oceanogr.*, *53*, 105–114.

Bond, N. A., J. E. Overland, M. Spillane, and P. Stabeno (2003), Recent shifts in the state of the North Pacific, *Geophys. Res. Lett.*, *30*(23), 2183, doi:10.1029/2003GL018597.

Bourassa, M., D. Legler, J. O'Brien, and S. Smith (2003), SeaWinds validation with research vessels, *J. Geophys. Res.*, *108*(C2), 3019, doi:10.1029/2001JC001028.

Cox, M., and K. Bryan (1984), A numerical model of the ventilated thermocline, *J. Phys. Oceanogr.*, *14*, 674–687.

Crawford, W., J. Y. Cherniawsky, and M. G. Foreman (2000), Multi-year meanders and eddies in Alaskan Stream as observed by TOPEX/Poseidon altimeter, *Geophys. Res. Lett.*, *27*(7), 1025–1028.

Crawford, W., P. Sutherland, and P. van Hardenberg (2005), Cold water intrusion in the eastern Gulf of Alaska in 2002, *Atmos. Ocean*, *43*(2), 119–128.

DaSilva, A., C. Young, and S. Levitus (1994), *Atlas of Surface Marine Data, NOAA Atlas NESDIS 6*, Nat. Oceanic and Atmos. Admin., Silver Spring, Md.

Dever, E., and C. Winant (2002), The evolution and depth structure of shelf and slope temperatures and velocities during the 1997–1998 El Niño near Point Conception California, *Prog. Oceanogr.*, *54*, 77–103.

Ducet, N., P. L. Traon, and G. Reverdin (2000), Global high-resolution mapping of ocean circulation from TOPEX/Poseidon and ERS-1 and -2, *J. Geophys. Res.*, *105*(C8), 19,477–19,498.

Durazo, R., and T. Baumgartner (2002), Evolution of oceanographic conditions off Baja California: 1997–1999, *Prog. Oceanogr.*, *54*, 7–31.

ETOPO5 (1988), Digital relief of the surface of the Earth, *Data Announce. 88-MGG-02*, Natl. Geophys. Data Cent., Boulder, Colo.

Fairall, C. W., E. Bradley, J. Godfrey, J. Wick, and G. Young (1996a), Cool-skin and warm-layer effects on sea surface temperature, *J. Geophys. Res.*, *101*(C1), 1295–1308.

Fairall, C. W., E. Bradley, D. Rogers, J. Edson, and G. Young (1996b), Bulk parameterization of air-sea fluxes for tropical ocean-global atmosphere coupled-ocean atmosphere response experiment, *J. Geophys. Res.*, *101*(C2), 3747–3764.

Freeland, H. J., G. Gatien, A. Huyer, and R. Smith (2003), A cold halocline in the northern California Current: An invasion of subarctic water, *Geophys. Res. Lett.*, *30*(3), 1141, doi:10.1029/2002GL016663.

Haidvogel, D. B., H. G. Arango, K. Hedstrom, A. Beckmann, P. Malanottte-Rizzoli, and A. F. Shchepetkin (2000), Model evaluation experiments in the North Atlantic basin: Simulations in nonlinear terrain-following coordinates, *Dyn. Atmos. Oceans*, *32*, 239–281.

Hare, S., and R. Francis (1995), Climate change and salmon production in the northeast Pacific ocean, in *Ocean Climate and Northern Fish Populations*, edited by R. Beamish, *Can. Spec. Publ. Fish. Aquat. Sci.*, *121*, 357–372.

Huyer, A., and R. L. Smith (1985), The signature of El Niño off Oregon, 1982–1983, *J. Geophys. Res.*, *90*, 7133–7142.

Huyer, A., R. Smith, and J. Fleishbein (2002), The coastal ocean off Oregon and northern California during the 1997–8 El Niño, *Prog. Oceanogr.*, *54*, 311–341.

Kalnay, E., et al. (1996), The NCEP/NCAR 40-year reanalysis project, *Bull. Am. Meteorol. Soc.*, *77*, 437–471.

Kaplan, A., M. A. Cane, D. Chen, D. L. Witter, and R. Cheney (2004), Small-scale variability and model error in tropical Pacific sea level, *J. Geophys. Res.*, *109*, C02001, doi:10.1029/2002JC001743.

Kosro, P. (2002), A poleward jet and an equatorward undercurrent observed off oregon and northern California during the 1997–98 El Niño, *Prog. Oceanogr.*, *54*, 343–360.

Ladd, C., N. Kachel, C. Mordy, and P. Stabeno (2005), Observations from a Yakutat eddy in the northern Gulf of Alaska, *J. Geophys. Res.*, *110*, C03003, doi:10.1029/2004JC002710.

Large, W., J. McWilliams, and S. Doney (1994), Oceanic vertical mixing: A review and a model with a nonlocal k-profile boundary layer parameterization, *Rev. Geophys.*, *32*(4), 363–403.

Levitus, S., and T. Boyer (1994), *World Ocean Atlas 1994*, vol. 4, *Temperature, NOAA Atlas NESDIS 4*, Natl. Oceanic and Atmos. Admin., Silver Spring, Md.

Levitus, S., R. Burgett, and T. Boyer (1994), *World Ocean Atlas 1994*, vol. 3, *Salinity, NOAA Atlas NESDIS 3*, Natl. Oceanic and Atmos. Admin., Silver Spring, Md.

Malanottte-Rizzoli, P., K. Hedstrom, H. Arango, and D. Haidvogel (2000), Water mass pathways between the subtropical and tropical ocean in a climatological simulation of the North Atlantic ocean circulation, *Dyn. Atmos. Oceans*, *32*, 331–371.

Mantua, N., S. Hare, Y. Zhang, J. Wallace, and R. Francis (1997), A Pacific interdecadal climate oscillation with impacts on salmon production, *Bull. Am. Meteorol. Soc.*, *78*, 1069–1079.

Marchesiello, P., J. C. McWilliams, and A. Shchepetkin (2001), Open boundary conditions for long-term integration of regional ocean models, *Ocean Modell.*, *3*, 1–20.

Mellor, G. L., and T. Yamada (1982), Development of a turbulence closure for geophysical fluid problems, *Rev. Geophys.*, *20*(4), 851–875.

Milliff, R. F., W. G. Large, J. Morzel, G. Danabasoglu, and T. Chin (1999), Ocean general circulation model sensitivity to forcing from scatterometer winds, *J. Geophys. Res.*, *104*(C5), 11,337–11,358.

Moore, A. M., H. G. Arango, A. J. Miller, B. D. Cornuelle, E. D. Lorenzo, and D. Neilson (2004), A comprehensive ocean prediction and analysis system based on the tangent linear and adjoint components of a regional ocean model, *Ocean Modell.*, *7*, 227–258.

North Pacific Marine Science Organization (PICES) (2005), Report of the study group on fisheries and ecosystem response to recent regime shifts, *Sci. Rep. 28*, N. Pac. Mar. Sci. Org. (PICES), Sidney, B.C., Canada. http://www.pices.int/, editor: J. R. King.

Pedlosky, J. (1987), *Geophysical Fluid Dynamics*, 2nd ed., Springer, New York.

Peterson, W. T., and F. B. Schwing (2003), A new climate regime in northeast Pacific ecosystems, *Geophys. Res. Lett.*, *30*(17), 1896, doi:10.1029/2003GL017528.

Powell, T. M., C. V. Lewis, E. N. Curchitser, D. B. Haidvogel, A. J. Hermann, and E. L. Dobbins (2005), Results from a three-dimensional, nested biological-physical model of the California Current System and comparisons with statistics from satellite imagery, *J. Geophys. Res.*, doi:10.1029/2004JC002506, in press.

Rayner, N., D. Parker, E. Horton, C. Folland, L. Alexander, D. Rowell, E. Kent, and A. Kaplan (2003), Global analyses of sea surface temperature, sea ice, and night marine air temperature since the late nineteenth century, *J. Geophys. Res.*, *108*(D14), 4407, doi:10.1029/2002JD002670.

Royer, T. C. (1985), Coastal temperature and salinity anomalies in the northern Gulf of Alaska, 1970–84, in *El Niño North*, edited by W. Wooster and D. Fluharty, pp. 185–187, Univ. of Wash., Seattle.

Shchepetkin, A. F., and J. C. McWilliams (1998), Quasi-monotone advection schemes based on explicit locally adaptive dissipation, *Mon. Weather Rev.*, *126*, 1541–1580.

Shchepetkin, A. F., and J. C. McWilliams (2003), A method for computing horizontal pressure-gradient force in an oceanic model with a nonaligned vertical coordinate, *J. Geophys. Res.*, *108*(C3), 3090, doi:10.1029/2001JC001047.

Shchepetkin, A. F., and J. C. McWilliams (2005), The Regional Ocean Modelling System: A split-explicit free-surface, topography-following coordinate ocean model, *Ocean Modell.*, *9*, 347–404.

Song, Y., and D. Haidvogel (1994), A semi-implicit ocean circulation model using a generalized topography-following coordinate system, *J. Comput. Phys.*, *115*, 228–244.

Strub, P., and C. James (2002), Altimeter-derived surface circulation in the large-scale NE Pacific gyres: Part 2: 1997–1998 El Niño, *Prog. Oceanogr.*, *53*, 185–214.

Umlauf, L., and H. Burchard (2005), A generic length-scale equation for geophysical turbulence models, *J. Mar. Res.*, in press.

Ware, D., and R. Thomson (2000), Interannual to multidecadal timescale climate variations in the northeast Pacific, *J. Clim.*, *13*, 3209–3220.

Warner, J. C., C. R. Sherwood, B. Butman, H. Arango, and R. P. Signell (2005), Performance of four turbulence closure models implemented using a generic length scale method, *Ocean Modell.*, *8*, 81–113.

Wentz, F., D. Smith, C. Mears, and C. Gentemann (2001), Advanced algorithms for QuikSCAT and SeaWinds/AMSR, paper presented at IGARSS'01, Inst. of Electr. and Electron Eng., Sydney, N.S.W., Australia.

E. N. Curchitser and A. Kaplan, Lamont-Doherty Earth Observatory of Columbia University, 61 Route 9W, Palisades, NY 10964, USA. (enrique@ldeo.columbia.edu; alexeyk@ldeo.columbia.edu)

E. L. Dobbins and A. J. Hermann, Joint Institute for the Study of the Atmosphere and Ocean, University of Washington, P.O. Box 357941, Seattle, WA 98195, USA.

D. B. Haidvogel, Institute for Marine and Coastal Sciences, 71 Dudley Road, New Brunswick, NJ 08855, USA.

T. M. Powell, Department of Integrative Biology, University of California at Berkeley, Berkeley, CA 94720, USA.